

Improving the understanding of transient electromagnetic signals for near-surface applications by assessing the turn-off ramp

Lukas Aigner, 00926642

Advisor: Ass. Prof. Adrián Flores Orozco

16.10.2019

Danksagung

Zuallererst möchte ich mich bei Adrián Flores Orozco, sowohl für die Betreuung, als auch für die Gelegenheit mich an vielen geophysikalischen Forschungsprojekt zu beteiligen, bedanken. Der Dank für die ursprüngliche Idee sich mit der Rampenzeit des TEM-FAST System auseinander zu setzen gebührt Matthias Bücker. Bei beiden Betreuern möchte ich mich natürlich auch für die Zeit, die wir gemeinsam in Diskussion über das TEM Verfahren verbracht haben, bedanken.

Mein Dank gilt auch Timea, Theresa, Matthias und Jakob, die mich nicht nur bei der Arbeit im Feld sondern auch bei Python Fragestellungen und mit hilfreichen Tipps beim Verfassen der Arbeit unterstützt haben. Außerdem möchte ich mich bei Anton Lettenbichler für die großartige Unterstützung bei den Oszilloskop Messungen und den Erklärungen betreffend elektrotechnischer Hintergründe bedanken. Zusätzlich auch ein herzliches Danke, an Walter Loderer für die Unterstützungen mit der Bestellung von Messequipment und jede Art von technischer Beratung. Des Weiteren möchte ich mich auch bei Fritz Punter für die Einführung in die Welt von \LaTeX bedanken, ohne die ich mich am Ende wahrscheinlich fürchterlich mit Word geärgert hätte.

Natürlich gilt mein Dank auch meinen Eltern, die nicht nur mein Studium ermöglichten, sondern mich auch ansonsten immer unterstützen. Zu guter Letzt bedanke ich mich auch bei Lisa, die den absoluten Großteil meiner Frustration abbekommen hat, wenn ich mal wieder tagelang nichts weiterbekommen habe.

Contents

1	Introduction	11
1.1	Motivation and background	11
1.2	Research objectives	12
1.3	Petrophysical relationships	12
2	Methods	15
2.1	Electromagnetic Methods	15
2.1.1	Time-domain or transient electromagnetic method	15
2.1.2	Frequency domain methods	19
3	Processing of geophysical methods	22
3.1	Introduction	22
3.2	Transient electromagnetic method	22
3.2.1	Introduction	22
3.2.2	Processing of an individual sounding	23
3.2.3	Batch processing of numerous soundings	24
3.2.4	Practical operation and inversion	25
3.3	Electromagnetic method at low induction number	28
3.4	Electrical resistivity tomography	29
3.5	Seismic refraction tomography	30
4	Assessment of the turn-off ramp of TEM soundings	32
4.1	Introduction	32
4.1.1	Background and motivation	32
4.1.2	Objective	32
4.1.3	Forward modeling to emphasize the importance	33
4.2	Methodology and measurements	33
4.2.1	Basic measurement concept and signal structure	33
4.2.2	Oscilloscope measurements	37
4.3	Results	39
4.3.1	Signal structure	39
4.3.2	Quantification of the length of the turn-off ramp	42
4.3.3	Results and discussion	44
4.4	Influence of the turn-off time on inversion results	45
4.5	Conclusion	50

5	Investigation of a brick-clay resource using electromagnetic methods to quantify clay content	51
5.1	Introduction	51
5.1.1	Background and Motivation	51
5.1.2	Objective	51
5.1.3	Study area	52
5.2	Field measurements	52
5.3	Transient electromagnetic data processing	53
5.4	Results and interpretation	56
5.4.1	Transient electromagnetics	56
5.4.2	Electromagnetic profiling	56
5.4.3	Electrical resistivity tomography	57
5.5	Conclusion	59
6	Characterization of a clayey landslide by integral application of multiple geophysical and geotechnical methods	60
6.1	Introduction	60
6.1.1	Background and Motivation	60
6.1.2	Objectives	60
6.1.3	Study area	61
6.2	Field measurements	62
6.3	Transient electromagnetic data processing	63
6.4	Results	64
6.4.1	Transient electromagnetic measurements	64
6.4.2	Electromagnetic method at low induction number - Mapping . . .	69
6.4.3	Electrical resistivity and seismic refraction tomography for validation of the transient electromagnetic results	70
6.5	Comparison to geotechnical methods and interpretation	73
6.6	Conclusion	75
7	Conclusion	77
	Bibliography	78

List of Figures

1.1	Conceptual model of the 3 conduction mechanisms, adapted as seen in a lecture by Adrián Flores Orozco. The image in the background is a thin section of sandstone and was taken from Paxton 2016.	12
1.2	Overview of the range of typical resistivity values from geological media. Taken from Gonzalez-Alvarez 2014.	14
2.1	Measurement principle of the TEM method from Bücken et al. 2017. All measurements presented within this work were done using the same loop for transmitting	17
2.2	Conceptual model of two consecutive pulses adapted from Christiansen, Auken, and Sørensen 2006, p. 189 to resemble the unipolar pulses used by the TEM-fast system.	18
2.3	Measurement principle of the EMI method from Boaga 2017.	20
3.1	An example of a filtered data taken from chapter 5. The grey diamonds indicate the position of those measurement points, which were removed before the inversion.	24
3.2	ZondTEM menu to control inversion parameters. The screenshot shows the inversion setup, to produce the results shown in the case studies of this work.	26
4.1	Forward modeling results calculated with ZondTEM software for a homogeneous 10 Ωm model.	34
4.2	Forward modeling results calculated with ZondTEM software for a homogeneous 100 Ωm model.	35
4.3	Forward modeling results calculated with ZondTEM software for a homogeneous 10000 Ωm model.	36
4.4	Time division in horizontal direction; voltage division in vertical direction and the trigger level is indicated by the gray dashed line. The picture in the background is from another oscilloscope, which is able to save screenshots - courtesy of Anton Lettenbichler.	38
4.5	Circuit diagram of the oscilloscope measurements. (created using Scheme-it online tool from https://www.digikey.at/schemeit/)	39
4.6	Full measurement cycle for a single stack of the TEM-fast system. It consists of a train of 17 bursts.	40
4.7	One of the 17 bursts of a stack. It consists of 63 single pulses.	41
4.8	Two subsequent parts of two of the total 63 pulses.	41

4.9	Zoom to the moment in time where the current is cut off. The voltage is limited to 20 V by the input stage of the oscilloscope.	42
4.10	Voltage peak, after the current is shut off. The first red line (t_0) indicates the moment in time where the shut-off process is started. The other three red lines (t_1 , t_2 and t_3) mark the positions where the signal level drops back / crosses the initial signal level and represent possible turn-off times.	43
4.11	Conceptual model of two consecutive pulses adapted from Christiansen, Auken, and Sørensen 2006, p. 189 to emphasize the relation between the width of the voltage peak of the electromotive force and the turn-off time.	44
4.12	Comparison of two turn-off time measurements for a 6 m loop (25 m cable) at two different sites, with significant differences in subsurface electrical resistivity.	45
4.13	Comparison of two turn-off time measurements with two different loop sizes (12.5 m and 25 m) at 4 A.	46
4.14	Comparison of two turn-off time measurements with two different current levels using a 12.5 m loop (50 m cable).	47
4.15	Comparison of two turn-off time measurements with a single turn (6 m side length) and 4 turns (3 m side length) using a 25 m cable.	48
4.16	Changes in inversion results due to different turn-off ramp lengths. Inversions were calculated with ZondTEM for an exemplary data set measured with a 25 m loop and 4 A current.	49
4.17	Sub-menu of the zondTEM software to control the TEM-pulse parameters.	50
4.18	Header and some rows of data of a .tem data file. The parameter "deff" is set as the forward ramp parameter in zondTEM automatically.	50
5.1	Overview of the study area, the purple area indicates the existing brick-clay pit, the orientation of the geophysical profiles is indicated by the black arrow.	52
5.2	Representation of the full TEM data set in terms of the measured signal.	55
5.3	Representation of the full TEM data set in terms of the apparent resistivity.	55
5.4	Raw data and forward modeling response of the resistivity/depth model on the right. The top left subplot shows the model response in terms of the apparent resistivity and the subplot below in terms of the measured secondary magnetic field.	55
5.5	TEM section, starts at 6.25 m offset regarding the ERT-profile	56
5.6	EMI measurement in terms of electrical conductivity [mS/m]; The blue curves show the electrical conductivity at 2.2 m, 4.2 m and 6.7 m (Cond1, 2 and 3); The red lines show the in-phase part, at the same depths.	57
5.7	Comparison of EMI measurements obtained in two different directions along the profile for different coil separation resulting in 3 exploration depths.	57
5.8	ERT-section at 1.0 Hz; the subplot on the right side show the comparison to the TEM measurement at this position.	58

5.9	Direct comparison of the resistivity 1D-log obtained by the TEM method and the ERT method at two different positions along the profile.	58
5.10	Direct comparison of the percentual clay content and the electrical resistivity from the TEM method.	59
6.1	Overview of the Kreisbach study area. The border of the landslide is indicated by the black scarp line.	61
6.2	Representation of the full TEM data set in terms of the measured signal.	63
6.3	Representation of the full TEM data set in terms of the apparent resistivity.	63
6.4	Raw data and forward modeling response of the resistivity/depth model on the right. The top left subplot shows the model response in terms of the apparent resistivity and the subplot below in terms of the measured secondary magnetic field.	64
6.5	TEM-section along Line 2. The location is partly identical with ERT and SRT profile QP2 6.1 and starts at TEM-sounding number 11. The line ends with TEM-sounding number 20 in the west. The distance is chosen according to the distance along the QP2 ERT profile.	65
6.6	TEM-section along line 6. This line starts in the west of Figure 6.1 at TEM-sounding number 7 and ends with TEM-sounding number 48 in the east.	65
6.7	TEM-section along line 10. This line starts in the west of Figure 6.1 at TEM-sounding number 86 and ends with TEM-sounding number 80 in the east.	66
6.8	TEM – soundings along LP1 (ERT profile). This line starts in the south of Figure 6.1 at TEM-sounding number 1 and ends with TEM-sounding number 15 in the north. The distance is chosen according to the distance along the LP1 ERT profile.	66
6.9	2-D interpolation of the TEM 1-D models at selected depths. The black dots are indicating the center of sounding positions.	68
6.10	Raw-data plot of EMI line 13, which is exemplary of a clean measurement.	69
6.11	Raw-data plot of EMI line 11, which reveals the influence of parallel TEM-measurements at the end of the line.	69
6.12	Comparison of EMI maps (top row), to TEM maps (bottom row), and to a hill-shaded topographic map (top right subplot).	70
6.13	ERT profile qp2. The subplot on the right shows a comparison to a TEM sounding.	71
6.14	ERT profile lp1. The subplot on the right shows a comparison to a TEM sounding.	71
6.15	A comparison of results from ERT (top left subplot), SRT (bottom left subplot) and TEM measurements (right subplots) along QP2.	72
6.16	A comparison of results from geotechnical methods (1st and 2nd subplots) to geophysical methods (3rd and 4th subplot).	74

List of Tables

1.1	P-Wave velocities of different sediments and sedimentary rocks from Knödel, Krummel, and Lange 2013 complemented with the velocity of water and air.	14
4.1	An overview on how the Time-Key is affecting the timing and signal structure of the transmitted pulses. Adapted from the TEM-fast manual, by using a 3:1 ratio on the Ton+Toff time.	37
4.2	An overview of all measured turn-off times for multiple loop and system configurations.	46
5.1	The grain size distribution at the outcrop closest to the start of the geophysical section.	54

The application of the transient electromagnetic (TEM) method to near surface problems depends mainly on the correct resolution of shallow subsurface layers. To resolve the near-surface layers using the TEM method, it is necessary to adjust the obtained signals using correct turn-off ramp times. Hence, the main aim of this work is the quantification of the turn-off ramp. Furthermore, the ramp times are applied to improve the inversion results for determining correct electrical resistivity logs. Additionally, two case studies with a focus on near surface problems are presented to evaluate the corrected TEM resistivity logs. Within the first case study a brick-clay deposit is investigated to quantify the clay content in the subsurface. The aim of the second case study is to develop a novel methodology to characterize a clayey landslide. The quantification of the turn-off ramp was done by using an oscilloscope to measure the signals within the transmitter loop. The brick clay deposit is investigated using electric and electromagnetic methods and the results are validated by comparison to the clay content measured from in-situ soil samples. The development of a novel methodology to characterize a clayey landslide is based upon the integral application of geophysical and geotechnical methods. By application of seismic refraction tomography, it was possible to delineate unconsolidated areas in the subsurface, while the electrical and electromagnetic methods were able to discriminate between different lithological units. The evaluation of the, in terms of the turn-off ramp, corrected TEM resistivity logs was successful, since the TEM method was able to obtain similar results as the well-established electrical resistivity method. The oscilloscope measurements were repeated at different sites and for multiple measurement configurations to provide a data base of turn-off ramp times, ranging between 0.1 and 10 μs .

Die Anwendung der geophysikalischen Methode der transienten Elektromagnetik (TEM) auf oberflächennahe Fragestellungen ist insbesondere auf die korrekte Auflösung der seichtesten Untergrundstrukturen angewiesen. Um diese seichten Untergrundstrukturen mit der TEM Methode auflösen zu können, ist es notwendig die gemessenen Signale mit der korrekten Rampenzeit zu korrigieren. Daher ist das Hauptziel dieser Arbeit die Quantifizierung der Rampenzeit. Außerdem wird die Rampenzeit verwendet, um den Einfluss auf die Inversionsergebnisse zu verdeutlichen, sowie diese Ergebnisse zu verbessern. Zusätzlich wurden zwei Fallstudien mit Fokus auf oberflächennahe Anwendungen durchgeführt, um die verbesserten Inversionsergebnisse zu evaluieren. Im Zuge der ersten Fallstudie wurde eine Tonlagerstätte mit elektrischen und elektromagnetischen Methoden untersucht, um den Tongehalt des Untergrunds zu bestimmen. Die zweite Fallstudie hat es zum Ziel eine neue Methodik zur Charakterisierung von tonigen Hangrutschungen zu entwickeln. Die Rampenzeit der TEM Methode wurde durch Anwendung von Oszilloskopmessungen bestimmt. Der Untergrund der Tonlagerstätte wurde mit elektrischen und elektromagnetischen Methoden untersucht, und die Ergebnisse wurden mit dem aus Bodenproben bestimmten Tongehalt verglichen. Die neue Methodik zur Charakterisierung von tonigen Hangrutschungen basiert auf der gemeinsamen Anwendung von mehreren geophysikalischen und geotechnischen Methoden. Mit Hilfe der seismischen Refraktionstomographie (SRT) war es möglich, nicht konsolidierte Untergrundschichten zu erkennen, während es mittels geoelektrischer und elektromagnetischer Methoden möglich war, zwischen verschiedenen lithologischen Einheiten zu unterscheiden. Die Evaluierung der, mittels korrekter Rampenzeiten, korrigierten TEM Ergebnisse war erfolgreich, da die TEM Methode ähnliche Ergebnisse wie die etablierte geoelektrische Methode lieferte. Die Oszilloskopmessungen wurden an geologisch unterschiedlichen Standorten und mit verschiedenen Messkonfigurationen wiederholt, um eine Tabelle mit korrekten Rampenzeiten zu erhalten. Die gemessenen Rampenzeiten liegen in einem Bereich von 0.1 bis 10 μs .

1 Introduction

1.1 Motivation and background

The transient electromagnetic method is a geophysical method capable of determining the subsurface electrical resistivity as a function of depth. According to the comprehensive review by Christiansen, Auken, and Sørensen 2006 the transient electromagnetic method was designed and developed during the 1980's mainly for mineral exploration of deep reservoirs. Within the last couple of decades the TEM method has also found an increasing application to solve near-surface problems such as hydrological and geological problems (e.g Bucker et al. 2017, Danielsen et al. 2003). Additionally, airborne TEM measurements are used frequently for geological mapping of large areas and for mineral exploration. A recent study by Auken et al. 2018 presents the ability of a newly developed towed TEM system to efficiently map large areas down to a depth of 70 m.

Another geophysical method, that is also capable of determining the subsurface electrical resistivity is the electrical resistivity tomography (ERT) method. The ERT method is well established in investigating similar hydrological and geological problems with a superior lateral resolution, while even providing a 2-D image of the subsurface. However, the depth of investigation of the ERT method is limited by the profile length and is significantly lower at the borders of the 2-D section. Therefore, the TEM method might be able to aid with the resolution of deeper structures, especially in confined space. Furthermore, the TEM method does not require a galvanic contact to the ground. Additionally, the TEM-FAST 48 system, used within this work, can be easily carried by a single person to even the most remote locations.

As described by Raiche 1984 and Fitterman and Anderson 1987 the turn-off ramp is a critical system parameter of the TEM method, controlling the correct measurement of early time data as well as the overall shape of the signal. In particular, early time data is important to correctly resolve near-surface structures. Typical TEM systems measure the turn-off ramp together with the data and provide it to the user to correct the measurements during data processing using any software package. The TEM-FAST 48 system, does not provide this information to the user. Therefore, it is necessary to measure the turn-off time of this TEM system, to correct TEM measurements. As far as the author is aware, there have been no published studies, that deal with the ramp and signal structure of the TEM-FAST system in particular.

1.2 Research objectives

The main objective of this study is to measure the turn-off ramp using an oscilloscope. The findings from this experiment should be used in a subsequent step to evaluate the influence on inversion results and to improve the 1-D resistivity models. Additionally, the TEM method was used within two case studies, namely an investigation of a brick-clay pit and a landslide investigation. These investigations were done to evaluate the capability regarding near surface application and to validate whether the findings from ramp measurements are capable of improving the resulting resistivity models.

1.3 Petrophysical relationships

The electromagnetic and electric methods, which have been applied within this study, are both sensitive to the electrical resistivity of subsurface materials. The electrical resistivity (ρ - unit: Ωm) or its inverse the electrical conductivity ($\sigma = 1/\rho$ - unit: S/m) are describing how well electrical current can flow through materials. There are 3 different possibilities via which electrical current can be conducted in the subsurface. Figure 1.1 shows a conceptual model of those 3 conduction mechanisms. All of those conduction

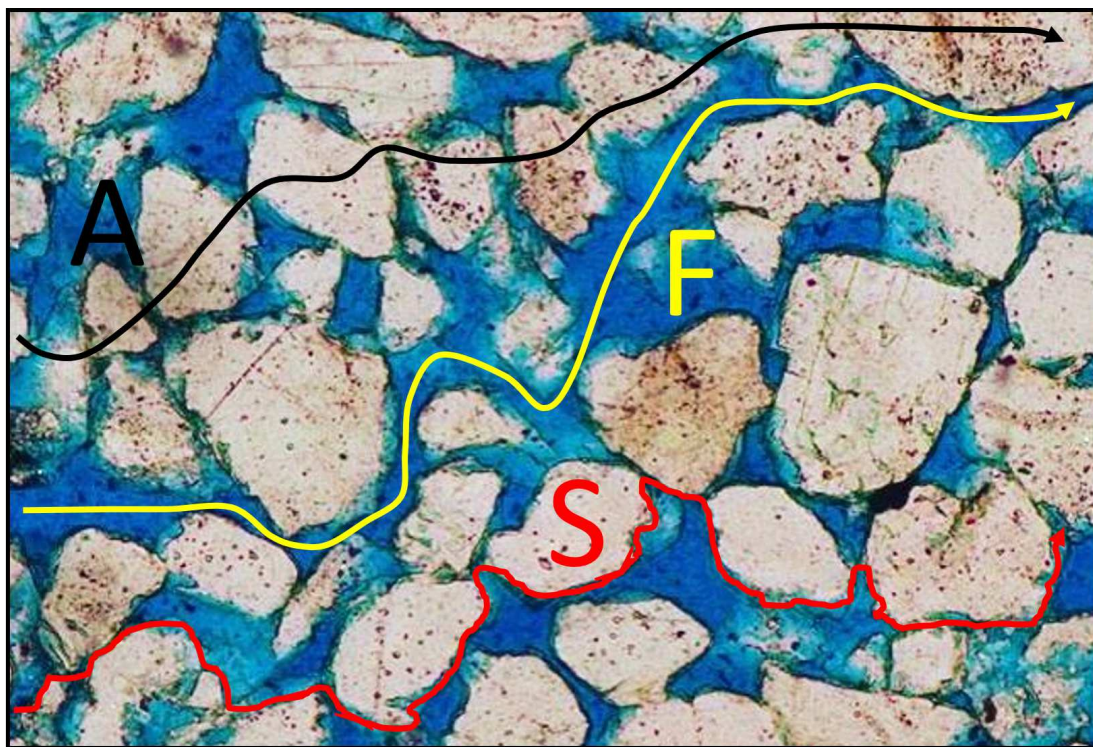


Figure 1.1: Conceptual model of the 3 conduction mechanisms, adapted as seen in a lecture by Adrián Flores Orozco. The image in the background is a thin section of sandstone and was taken from Paxton 2016.

mechanisms are present in parallel, although the magnitude of contribution from the individual parts varies greatly. For example, the “Matrix conduction” can be mostly neglected as long as there are no metallic minerals, or graphite present.

- Black line: Electrical conduction through grains and minerals (σ_A): “Matrix conduction”
- Yellow line: Electrical conduction in the fluid (σ_F): “Electrolytic conduction”
- Red line: Electrical conduction at the grain surface (σ_S): “Surface conduction”

According to Telford et al. 1990 most of the rock forming minerals, except for metallic minerals, are rather resistive to electric currents which pass through these media (“Matrix conduction”). The resistivity of geologic materials is lowered due to higher water content within the pores in case of sediments, or within fractures in case of rocks. The electric current is easily carried by ions dissolved in the pore water (“Electrolytic conduction”). Therefore, the electrical resistivity (ρ_0) is directly proportional to the fluid resistivity (ρ_f), while decreasing with material porosity (ϕ) and can be described by “Archie’s law” (Archie et al. 1942):

$$\rho_0 = a\rho_f\phi^{-m}S^{-n} \quad (1.1)$$

where the $-m$ exponent represents the cementation factor. The degree of pore saturation is described by S , and n is the saturation exponent. The parameter a is often referred to as tortuosity, which is a measure of how twisted a path through the pores is.

However, this empiric relationship holds only true if there is no clay present within the sediments of the subsurface. The presence of clay further decreases the electrical resistivity and can be explained by the high cation exchange capacity of clay minerals, due to current conduction via an electrical double layer along the fluid/mineral interface (eg. Waxman, Smits, et al. 1968). This electrical conduction mechanism is often referred to as interface or surface conduction (red line in figure 1.1). Figure 1.2 presents typical resistivity values of geological media.

To further evaluate the findings from electromagnetic methods the seismic refraction tomography (SRT) method was applied. The SRT method is capable of providing information on the seismic velocity distribution of the subsurface. Seismic velocities depend mainly on the density of the geological matter and an overview of typical velocity values for different geological material can be found in table 1.1. The velocity of subsurface material increases with increasing density but in case of sediments it is also dependent on porosity and saturation. Almost all of the parameters described in figure 1.2 and 1.1 are ranging over the order of a magnitude. Therefore, it is always good practice to apply multiple geophysical methods to reduce ambiguities.

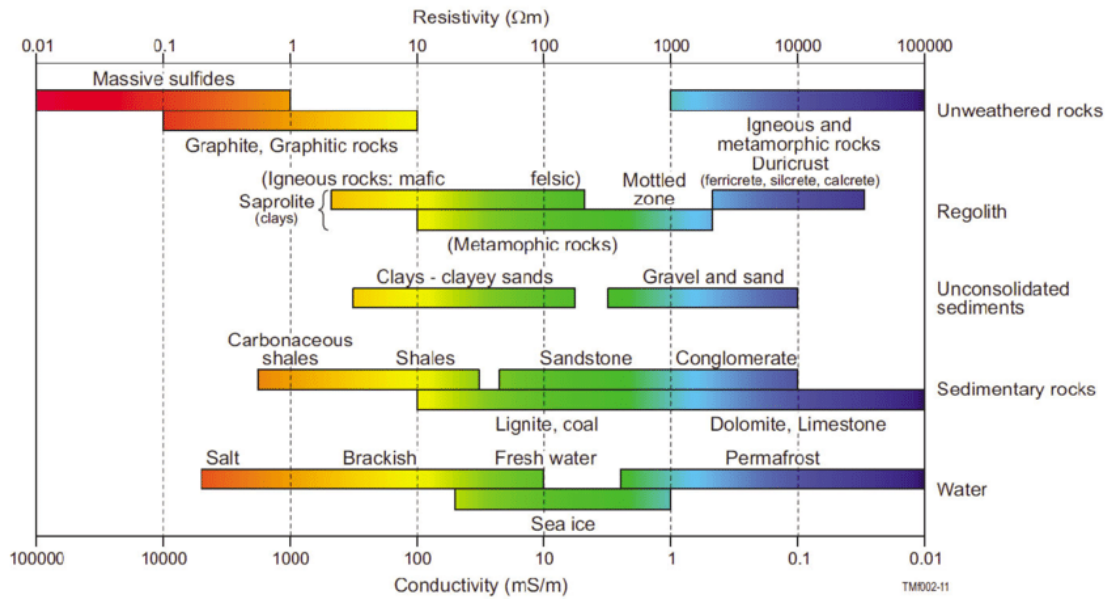


Figure 1.2: Overview of the range of typical resistivity values from geological media. Taken from Gonzalez-Alvarez 2014.

Table 1.1: P-Wave velocities of different sediments and sedimentary rocks from Knödel, Krummel, and Lange 2013 complemented with the velocity of water and air.

Geological material	P-Wave velocity [m/s]
Clay	1200-2800
- sandy clay	2000-2750
Sand (dry)	300-1500
- wet	200-2000
Gravel (dry)	180-550
- wet	750-1250
Marl	2000-4700
Sandstone	800-4500
Claystone	2200-4200
Water	1450
Air	330

2 Methods

This chapter provides an overview of the electromagnetic methods applied within this work. Further information on the TEM method can be found in Christiansen, Auken, and Sørensen 2006, while an in-depth description of the foundational theory was done by Ward and Hohmann 1988. Boaga 2017 provides a comprehensive review of the frequency domain electromagnetic methods, with a focus on hydrogeological problems.

Although this work focuses on the transient electromagnetic (TEM) method, other geophysical methods have been applied mainly to validate the findings using the TEM method. The ERT and SRT methods are only introduced briefly at the beginning of their respective processing sections and an extensive description can be found in most applied geophysics textbooks (e.g Everett 2013)

2.1 Electromagnetic Methods

Both electromagnetic methods applied within the scope of this work are based upon Faraday's law. Faraday's law states that an over time varying magnetic field will result in a rotating electric field, which can be expressed in differential form by formula 2.1.

$$\nabla \times \vec{E} = -\frac{\partial \vec{B}}{\partial t} \quad (2.1)$$

This relationship holds also true the other way around, meaning that a rotating electric field causes an over time varying magnetic field. This phenomenon will continue indefinitely in principal, although subsequent fields will decay rapidly in amplitude. These principles are applied by both the time-domain electromagnetic (TDEM) methods, and the frequency-domain electromagnetic (FDEM) methods. The difference lies in the physical reason for the change of the primary electric field. TDEM methods are using a direct current (DC) which is abruptly interrupted to generate an over time varying primary magnetic field. In contrast, FDEM methods are using an alternating current (AC) to generate an over time varying primary magnetic field. Further differences and the measurement principles of each of those methods are explained in 2.1.1 and 2.1.2 respectively.

2.1.1 Time-domain or transient electromagnetic method

Basic measurement principle

TDEM methods are commonly also called transient electromagnetic methods (TEM), since the method is measuring the decay of a secondary electromagnetic field, meaning

that this field is growing weaker until it cannot be measured anymore. The name TDEM methods was mainly used to point out the foundational difference to the FDEM methods. Throughout the remainder of this work the more common abbreviation “TEM” will be used.

The TEM method uses a direct current, which is passed through an ungrounded transmitter loop (Tx). This flow of current causes a static primary magnetic field. After the current is interrupted, the primary magnetic field consequently breaks down. Due to Faraday’s Law (2.1) this induces a secondary electrical field. This electrical field will cause a current flow in the subsurface. These, so called eddy currents will generate a secondary magnetic field, which can be measured at the surface. This measurement is done in terms of a voltage, that is induced by an electromotive force into a receiver loop (Rx) at the surface. The amplitude and the decay of the secondary magnetic field is dependent on the subsurface resistivity distribution. This process is slower for less resistive grounds, compared to high resistive subsurface materials, where the current system will decay faster.

Figure 2.1 shows a comprehensive illustration by Bucker et al. 2017, which is also presenting the orientation of the electromagnetic fields. It is also indicating that the induced eddy currents are moving outwards (away from the loop) as well as downwards. In fact, the current density’s maximum is diffusing about twice as much horizontally as vertically (Christiansen, Auken, and Sørensen 2006, p. 192). This diffusion of the current system is commonly referred to as a smoke ring, which is a fitting analogy. To achieve a reasonable field efficiency, the transmitter loop (Tx) is extended horizontally on the surface in a square, which is an appropriate approximation of the theoretical circle shape. The measurement is either done using a dedicated receiver loop (Rx) or the same loop that was used for transmitting the signal in the first place. The second option is called a coincident loop and can be done, because the primary field is already turned off, when the secondary field is measured.

The basic principle in terms of the amplitudes of the applied current, the induced electromotive force and the secondary magnetic field is presented in figure 2.2. The signal is measured using logarithmically increasing time windows, to enhance the signal to noise ratio at later times. According to Christiansen, Auken, and Sørensen 2006, p. 189 ground based systems use the following time ranges for the respective parts of the signal structure:

- Turn-on ramp: 50-200 μs
- ON-time: 1-40 ms
- Turn-off ramp: 1-40 μs
- OFF-time: 1-40 ms to measure the decay of the secondary magnetic field.

Further details on the signal structure of the measurement system used for this work can be found in 4.3.1. The current amplitude of the square wave form ranges from 1 A up to 50 A.

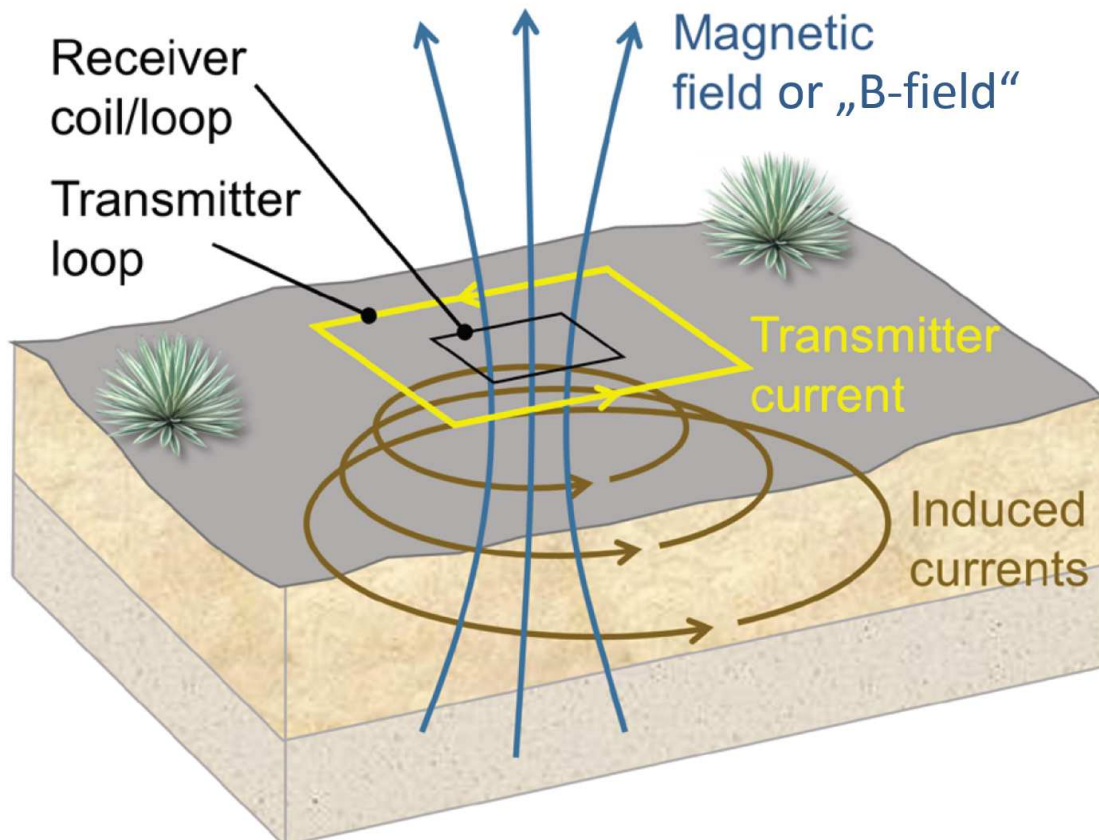


Figure 2.1: Measurement principle of the TEM method from Bückner et al. 2017. All measurements presented within this work were done using the same loop for transmitting .

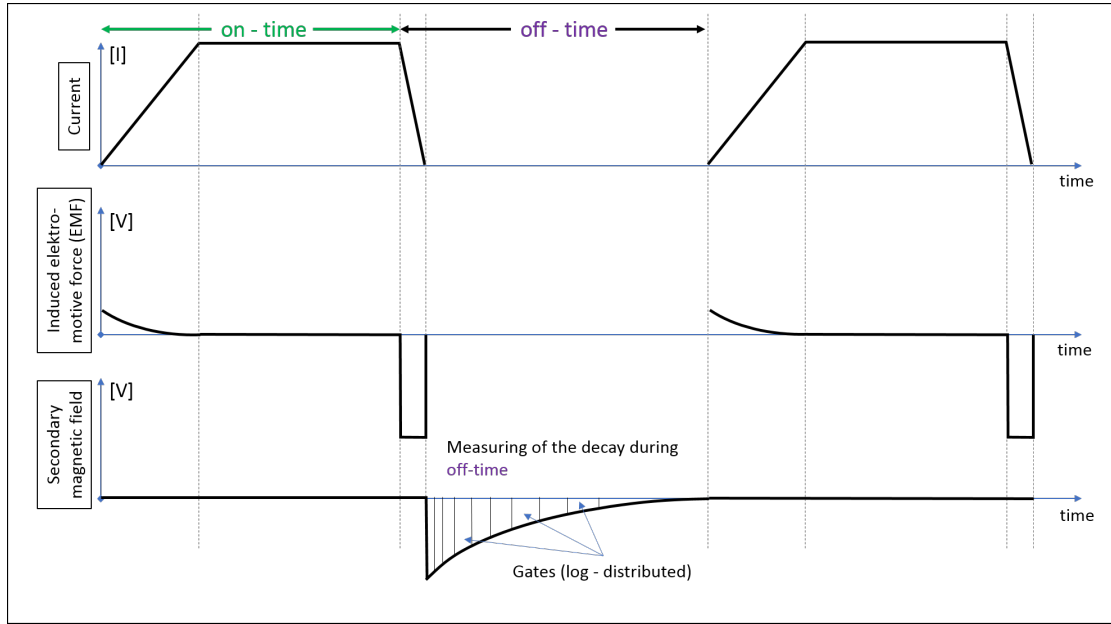


Figure 2.2: Conceptual model of two consecutive pulses adapted from Christiansen, Auken, and Sørensen 2006, p. 189 to resemble the unipolar pulses used by the TEM-fast system.

According to Spies 1989, the depth of investigation (DOI) of the TEM method is depending on three factors:

1. The electrical resistivity of the subsurface: Higher resistivity is decreasing DOI
2. The effective natural background noise level: Higher noise level is decreasing DOI
3. The magnetic moment of the transmitter loop: Higher magnetic moment is increasing DOI

Obviously, the first one cannot be influenced by the TEM operator, but as long as the reason for the noise remains mainly random it's effect can be reduced by additional stacking. However, the effect of additional stacking is limited, since a single stack of a TEM measurement already consists of between 1000 and 10000 individual soundings. Therefore, the most effective way to increase the DOI is to increase the magnetic moment of the transmitter loop, which is controlled by $M = nIa$.

- n ... the number of transmitter loop turns. M only increases, when the Tx side length stays constant, meaning that the cable length has to be doubled.
- I ... the current amplitude of the transmitter in ampere.
- a ... the area covered by the transmitter loop, controlled by the side length of the transmitter loop. This is a rather effective way to increase the magnetic moment, since doubling the cable length leads to a four time bigger area.

Another data representation: The late-time apparent resistivity

The decay of the secondary magnetic field is measured within the transmitter loop on the subsurface in terms of voltage. Another way to represent the measured data is to calculate the apparent resistivity. This is done because the visualization of the decaying magnetic field is not very informative (Christiansen, Auken, and Sørensen 2006, p. 196), while a plot of apparent resistivity is showing larger variations. The apparent resistivity is derived from the transient response of a homogenous half-space (Christiansen, Auken, and Sørensen 2006, p. 188) using a late time approximation:

$$\rho_a = \frac{1}{\pi} \left(\frac{M}{20 \frac{\partial b_z}{\partial t}} \right)^{\frac{2}{3}} \left(\frac{\mu_0}{t} \right)^{\frac{5}{3}} \quad (2.2)$$

The apparent resistivity (ρ_a) is dependent on the following parameters:

- $\frac{\partial b_z}{\partial t}$... impulse response in V measured at a certain time t .
- $M = nIa$... the magnetic moment of the transmitter, which is depending on the loop turns (n), the current amplitude (I in ampere) and the area covered by the transmitter loop (a in m^2).

An example of this visualization can be seen in figure 3.1, which shows, that the apparent resistivity enhances changes in the measured data. Therefore, it is recommended to use the apparent resistivity for filtering of the sounding curve as described in 3.2.2. It has to be noted, that the formula, implemented in the inversion software used within this work, is not described in the software manual and not known to the author.

2.1.2 Frequency domain methods

In comparison to the TEM method described above, FDEM methods use an alternating current at a particular frequency. The harmonic primary signal is transmitted into the subsurface using a transmitter coil (Tx). Similar to the TEM method, the over time changing primary magnetic field (H_p) causes the flow of eddy currents in the subsurface. These (secondary) eddy currents cause the secondary magnetic field (H_s) which is dependent on the conductivity of the soil. The receiver coil (Rx) measures the secondary field in two distinguishable parts, the so called in-phase (real - in-phase with the Tx signal) and out-of-phase (quadrature - 90 ° out-of phase of the Tx signal) part. Unlike the TEM method the measurements are obtained while the primary signal is transmitted. Figure 2.3 shows a representation of the measurement principle. The H_s field is in general a complicated function of the electromagnetic properties of the subsurface and the coil configuration. This relationship can be simplified if the measurement system is working on non-magnetic horizontally layered soil (Low induction number condition) and in the frequency range f of:

$$2\pi f \ll \frac{2}{\mu_0 \sigma s^2} \quad (2.3)$$

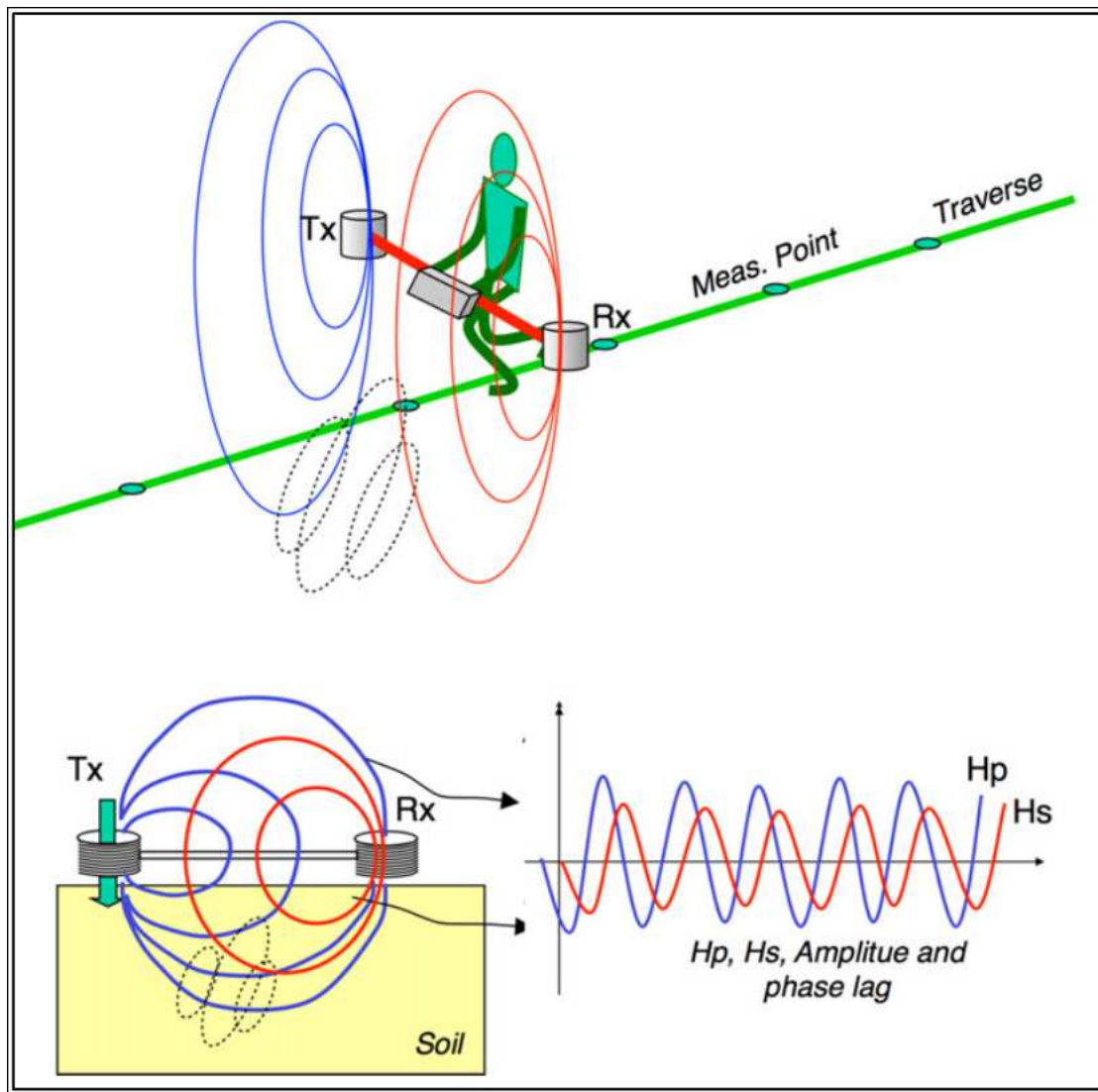


Figure 2.3: Measurement principle of the EMI method from Boaga 2017.

with μ_0 being the magnetic permeability of vacuum, σ the conductivity of the soil and s the spacing between the Tx and Rx coils. Therefore, FDEM methods using this simplification are often referred to as Electromagnetic methods at low induction number (EMI). According to Boaga 2017 the apparent ground conductivity is directly proportional to the ratio of the primary and secondary magnetic field as described by the following formula:

$$\sigma_a = \frac{4}{\omega \mu_0 s^2} \frac{H_s}{H_p} \quad (2.4)$$

with ω being the angular frequency. EMI equipment measures both parts of the signal, as described above. The in-phase ratio is measured in parts per thousand (ppt) and can be related to the magnetic susceptibility. High and inconstant values of the in-phase part are an indicator of magnetic materials in the subsurface. The out-of-phase ratio can be directly related to the apparent conductivity of the soil and is typically expressed in mS/m. To obtain an estimation of the true soil conductivity at depth it is necessary to invert the the apparent resistivity. However, the focus of this wok is on the TEM method. Therefore, a simple visualization of σ_a is sufficient, to reveal lateral changes of apparent soil conductivity. An additional visualization of the in-phase part is helpful to rule out the presence of magnetic materials (e.g metallic anthropogenic structures) in the subsurface.

3 Processing of geophysical methods

3.1 Introduction

The general processing of geophysical data can be divided in 4 main steps, of which not every step is necessary for all methods within this work:

1. Raw data visualization
2. Filtering of erroneous measurements
3. Inversion process
4. Evaluation of inversion results

The first step is necessary to gain insight into the data quality. Additionally, it is also used to filter the data set in the next step, while also providing a reference on how the filtering changed the measured data. The inversion process is necessary, if the geophysical problem cannot be solved directly from the data. Most geophysical problems are inverse problems, which means that there is no unique solution to the problem and that they suffer from an inherent ambiguity. This ambiguity is caused by the under determination of such problems, and because the measurements do not deliver exactly determined quantities. Therefore, the inversion process starts by comparing the forward response from an initial model, which is also called the predicted data, to the measured (also: observed) data. After that the model is adjusted and the forward model response is again compared to the measured data. This process is repeated iteratively until specific stopping criteria are met. After that the resulting model is visualized and it is compared to prior knowledge regarding the geological situation or to results from other geophysical measurements. Additionally, the first outcome should not be accepted without comparing it to equally possible solutions (resulting models). The following sections will describe the necessary processing steps for the geophysical methods applied within this work.

3.2 Transient electromagnetic method

3.2.1 Introduction

TEM data processing can be done either for individual soundings separately or for a bunch of soundings as batch processing. The most important step for both the individual and the batch processing is to eliminate all soundings affected by anthropogenic features. Anthropogenic features such as buried cables, power lines or fences exhibit a specific type of noise on the measured data, often called coupling noise. As described in Christiansen,

Auken, and Sørensen 2006, p. 205, there are two main coupling types. While capacitive coupling is mostly easy to recognize, due to its oscillating imprint on the data, galvanic coupling only shifts the sounding curve, without showing any typical imprint on the data. Therefore, galvanic coupling can only be recognized by comparing a sounding to other unaffected soundings in its vicinity. It has to be noted that it is highly advisable to keep a safe distance of at least 100 m to man-made conductors as described in detail in Christiansen, Auken, and Sørensen 2006, p. 204. Another way to identify buried man made conductors is to perform EMI measurements on the area of interest.

3.2.2 Processing of an individual sounding

The processing of an individual sounding is discussed first and can be divided into the following steps:

1. Remove all data points before or after a negative voltage reading is encountered.
2. Remove all data points before or after a discontinuous data point is encountered.
3. Run a first test inversion. If the data fit is acceptable and the resulting model plausible, the processing of an individual sounding is finished. If, either the data-fit or the resulting model is not sufficient, continue with the next step.
4. Remove more data points from either the beginning or the end of the sounding
5. Run another inversion and check if the data fit is improved and the resulting model is plausible. If not, re do iteratively from step 5 until an acceptable result is achieved.

It is highly recommended to visualize both the measured signal (voltage in the loop, caused by the secondary magnetic field) and the apparent resistivity. The expectation is that TEM sounding curves decay smoothly with time and do not show any sign reversal. There is one exception, which is the presence of induced polarization (IP) - effects on the data. This IP-effect on TEM measurements is described extensively in the work of Marchant 2015, but is not dealt with, within the scope of this work. Therefore, all negative voltage readings within a sounding are considered erroneous. To remain data continuity all data points (including the negative one) after the negative voltage reading are removed from the sounding curve. This holds only true if the data point is encountered in the latter part of the sounding curve (last third). If negative voltage readings are encountered in the first third of the sounding curve, only the data points before this point are removed. In the unlikely case, that a sounding with negative voltage readings all over the sounding curve, was not removed during the initial search for data affected by coupling noise, such a sounding will be removed entirely.

The expectation for the remaining curves is that both the voltage readings and the apparent resistivity are decaying smoothly over time. Data points, which deviate from the overall smooth decay or even show significant discontinuities are considered erroneous. Similarly to the handling of negative values, all points after (or/and before) including

the erroneous one are removed. An example of an individual sounding that has already been filtered can be seen in figure 3.1.

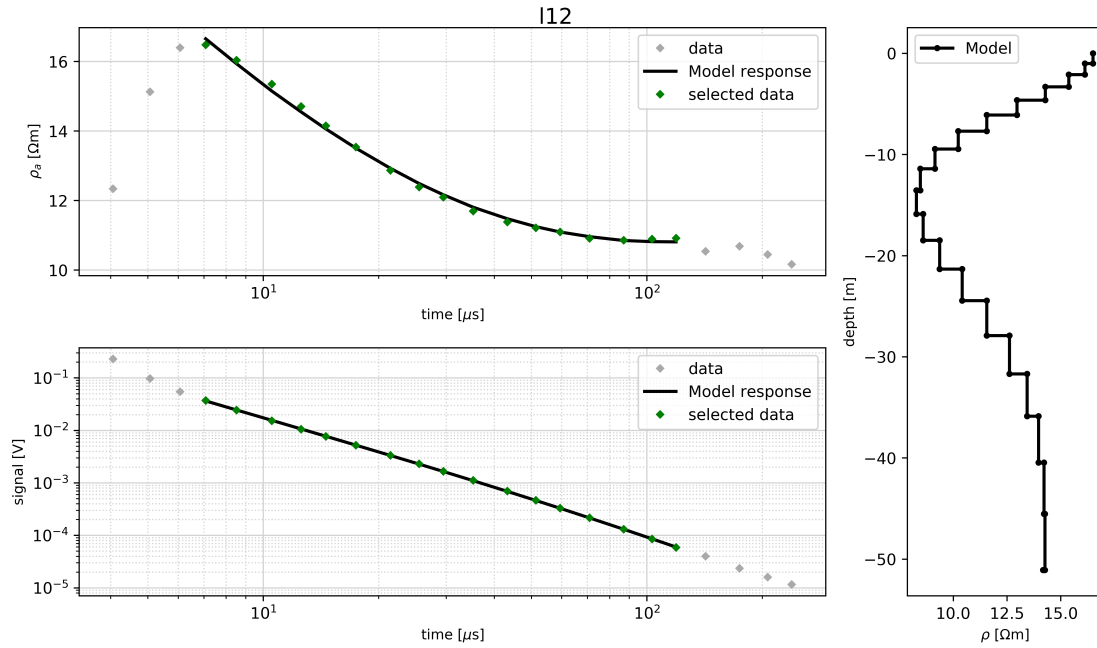


Figure 3.1: An example of a filtered data taken from chapter 5. The grey diamonds indicate the position of those measurement points, which were removed before the inversion.

The next step is to run a test inversion (described in detail below: 3.2.4) and check how well the resulting model represents the measured data (data-fit). If the data-fit is acceptable and the resulting model plausible, the TEM data processing for a single sounding is done and one can proceed with the next sounding. If the data-fit is insufficient, additional data points are removed from the sounding. The points are (similarly to the first two steps) removed one by one from the front or the back, depending on where the main data misfit is located along the sounding curve. After additional points are removed another inversion is done and the data-fit is checked again. This process is repeated iteratively until a fitting model is found, or too few points (<4) are left. The goal is to find the least complex model, which explains the data, while most of the data points remain part of the sounding curve. If no model, that adequately represents the data, can be found, the sounding has to be removed from the data. Such a sounding probably fell victim to unidentified coupling noise. The reader has to be aware that the implication does not hold true: A perfect data-fit does not mean that it is impossible that a sounding is affected by coupling noise.

3.2.3 Batch processing of numerous soundings

The batch processing of multiple soundings at once is mainly done to reduce the workload compared to processing each sounding individually. This process can be summarized by

the following steps:

1. Visualization of all soundings in a single view (“batch plot”).
2. Filtering of one of the smoothest sounding curves (“selected sounding”).
3. Inversion of the selected sounding to achieve a sufficient data-fit and a plausible model.
4. Apply the time range used for the inversion of the selected sounding to all soundings.
5. Inversion of the complete data. If the data-fit is acceptable and the resulting models are plausible, the batch processing is finished here.
6. (Optional) If necessary removal of additional data points from individual soundings and new inversion to improve the data-fit.

The first step is to visualize all soundings, which are going to be part of the batch processing, within a single plot (batch - plot). It is recommended, that only soundings from a single site are processed together. This batch-plot is used to select a sounding that is among the smoothest of all the sounding curves. This selected individual sounding is processed using the steps described above in 3.2.2. The time range, that was used to cut the individual sounding to achieve the (final) inversion result, is then used to cut all other sounding curves to the same time range. All soundings, which are now cut to a certain time range, are inverted one by one using the same initial model parameters and inversion settings as described in subsection 3.2.4. If the the data-fit, as well as the credibility of the resulting models are similar to the results from processing the selected sounding, the batch processing is finished here. All soundings that do not achieve a sufficient data-fit and plausible model, are further cut to narrower time ranges and a new inversion is started. This process is repeated until either an acceptable data-fit is achieved, or the sounding has to be removed entirely from the batch processing.

3.2.4 Practical operation and inversion

All raw data visualization presented within this work was done using the open source programming language PYTHON. In particular, the libraries numpy, pandas and matplotlib have proven to be valuable tools to visualize TEM data. Additionally, these tools have also been used to remove erroneous data points from a sounding curve as described above in 3.2.2. Consequently, also the batch pre-processing was done using Python and the associated tools mentioned above. Those steps can also be done interactively using the commercial software ZondTEM (Alex Kaminsky 2001), that was used for the data inversion. Unfortunately, ZondTEM does not highlight negative voltage readings explicitly in the raw data visualizations, which is why most of the pre-processing was done semi-automatically using PYTHON.

The inversion process itself was done using the commercial software ZondTEM (Alex Kaminsky 2001). Inversion with ZondTEM can be summarized by the following steps:

1. Additional pre-processing using the interactive graphical user interface.
2. Definition of an homogeneous initial model. Model depth \approx expected Depth of Investigation (DOI).
3. Setting of a few inversion parameters.

If necessary, additional points can be removed using the graphical user interface of ZondTEM. Inversion results from ZondTEM are mainly unaffected by the resistivity of the homogeneous initial model, if the data quality is high, meaning a smooth decay of the sounding curve. However, inversion results depend on the selection of an appropriate depth of the initial model. According to Bucker et al. 2017, p.283 a rule of thumb to estimate the depth of investigation is 2-3 times the loop diameter. After choosing an appropriate initial model depth some parameters for the inversion process itself have to be set. Within this work all soundings have been inverted using the settings as presented in figure 3.2. The inversion results produced within this work were also compared to results using different settings. The following list explains the most important parameters:

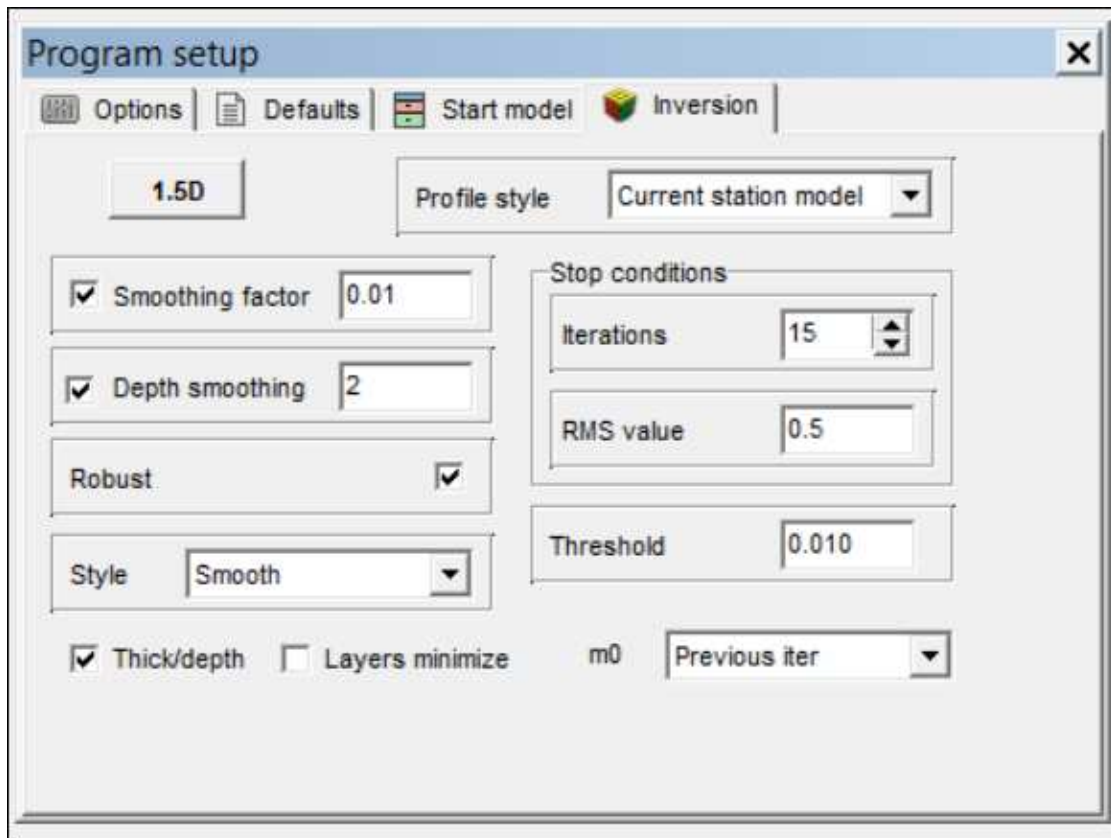


Figure 3.2: ZondTEM menu to control inversion parameters. The screenshot shows the inversion setup, to produce the results shown in the case studies of this work.

- Style: Smooth - A smoothness constrained inversion approach. This style was chosen mainly, because the inversion of ERT data, which was done to evaluate the results from TEM measurements, also relies on a smoothness constrained approach (3.4).
- Smoothing factor: An empirical parameter, depending mainly on the data quality. Since most measurements showed little to no influence of noise it was chosen rather low. For noisy data, this parameter can be increased up to 10.
- Stop conditions: Either the number of iterations, or the RMS error between the measured data and the calculated model response.

Further information can be found in the software manual available from Zond software corporation.

After the inversion is completed the results can be exported to an excel file, which can be read and visualized using the PYTHON libraries, which were already introduced above. In addition, the scipy (Jones, Oliphant, Peterson, et al. 2001) and pyKrige library (Murphy 2014) have been used for 1-D and 2-D interpolation purposes.

3.3 Electromagnetic method at low induction number

The processing of electromagnetic method at low induction number (EMI) data, that was done within the scope of this work is based on a simple visualization of the measured data. This was done using the open source programming language PYTHON, relying on the numpy, scipy (Jones, Oliphant, Peterson, et al. 2001), pandas and matplotlib libraries as well as on the pyKrige (Murphy 2014) package.

As described in 2.1.2 the data collected with the EMI system used within this thesis consists of the in-phase part and the out-of-phase part. While the in-phase parts do not contribute to the total conductivity of the soil, they are an important indicator of data quality and are therefore used to assure that no metallic structures interfere with the measurements. The out-of-phase part is proportional to the soil conductivity at a certain depth and can be calculated by using a proportionality factor. This factor can be estimated by calibration of the device prior to measuring.

The visualization itself was done either along selected profiles or for a 2-D area. The first case was achieved by simply plotting the conductivity versus the distance along the profile. The simplest way to achieve this is to use the XYZ-coordinates from a GPS-antenna, which can be connected to the CMD explorer or to the mini Explorer. Unfortunately during all measurements within this thesis the connection between GPS-antenna and EMI system wasn't operable. Therefore, a linear interpolation between markers at certain distances along the measured profiles was done to provide XYZ-coordinates for each measurement point. Those marker points were measured during EMI data acquisition using a Leica GPS system. The 2-D map was constructed by interpolating between all measurement points and visualizing the resulting equidistant points as a color coded contour map. Examples for both of these can be found in the upcoming case studies.

3.4 Electrical resistivity tomography

The electrical resistivity tomography (ERT) method uses a controlled current injection between two firmly grounded metal electrodes, while the voltage is measured at another pair of electrodes. By applying Ohm's law and taking the geometry of the electrodes into account an apparent resistivity of the measurement can be calculated. In case of a homogeneous subsurface the apparent resistivity is equal to the electrical resistivity of the subsurface. However, this is seldom the case and the electrical resistivity of the subsurface is varying laterally as well as vertically. Therefore, the distribution of subsurface resistivity can only be solved by means of inversion.

The first step to process ERT data is always the calculation of a so called pseudosection. A pseudosection is a representation of the measured data and presents the apparent electrical resistivity using a pseudodepth mapped to the distance along the measurement profile. A pseudosection is then used to eliminate obvious outliers, such as poorly-connected electrodes, from the data set. Additionally, all physically implausible measurements, such as negative current amplitudes were also removed from the data set. The data set was inverted using a smoothness constrained inversion algorithm "CRTomo", which was developed by (Kemna 2000). "CRTomo" is capable of fitting complex valued electrical resistivity data to a certain error level. To select an adequate error model a histogram is commonly used. The error model can be described by the following relationship (Slater et al. 2000):

$$\epsilon(R) = a + bR \quad (3.1)$$

where a is the absolute error (Ω), b the relative error (%) and R the transfer Resistance. Although the complex part of the electrical resistivity is not used within this work, the usage of the error level as a stopping criteria has proven to minimize the risk of artifacts in inversion results. The inversion results were visualized using adapted python scripts developed by Jakob Gallistl at TU Vienna. To limit the scope of this work, Adrián Flores Orozco provided the already processed and inverted datasets used within the following case studies.

3.5 Seismic refraction tomography

The seismic refraction tomography (SRT) is based on the propagation of elastic waves through the subsurface. The associated ground movement can be measured with seismic sensors. In engineering applications, the elastic waves are artificially generated (hammer blows, explosions) and recorded with so-called geophones. The observed ground motion waveforms permit to determine the travel time (indicated by the first onset) between shot position and geophone. Based on the known geometry of such survey layouts consisting of numerous shot and geophone positions the observed travel times can be used to solve for the seismic velocities in the subsurface by means of a tomographic inversion. The processing of refraction seismic data in terms of a tomography is based on three main steps:

1. Visualization of raw data and enhancement of the signal-to-noise ratio (SNR).
2. First break picking
3. Inversion

First of all the measured ground movements at each geophone for each shot have to be visualized. There are numerous different gathers possible, but within this work traces were gathered based on the shot index number. The shot index gather results in a seismogram for each individual shot, containing a number of traces equal to the number of geophones. Depending on the data quality and especially on the SNR it might be necessary to improve the visibility of the first onsets. This highlighting of the first onsets can be done by rescaling the amplitudes or by applying different frequency filters. After that, the picking of the first breaks can be done. Hereby, it is necessary to highlight the start of the first positive amplitude (usually visualized by a black-filled waveform). These first breaks, closest to the shot, are related to the progression of the direct wave until the direct wave is overtaken by the primary wave (P-wave). The progression of elastic waves through the subsurface is stored in terms of travel times between shot and geophone. All these steps can be done using a PYTHON software package called “ptseis” which was developed at TU Wien by Matthias Steiner. Ptseis is operated from a powershell and is capable of visualizing seismic records and their frequency spectrum. Furthermore, frequency filtering, amplitude scaling and visualization of theoretical velocity vectors is possible within the chosen data collection (such as: Shot, receiver and common offset collections). The first break picking is done within an interactive plot window and these “picks” can be exported together with the survey geometry in a format compatible to the inversion software (pyGIMLi - described below). A detailed description of all the commands and capabilities can be found in the software manual (available on request from Matthias Steiner).

The inversion process can be described as the search for a velocity model, which explains the measured travel times. This can be done using the refraction module of the open source geophysical modeling library pyGIMLi (Rücker, Günther, and Wagner 2017). The inversion process compares the measured travel times to theoretical traveltimes calculated

from possible wavepaths within the iteratively adapted initial model. The initial model can be parametrized within pyGIMLi using mesh tools to create a finite element grid on which the inversion is calculated. pyGIMLi uses a regularization parameter called lambda and the inversion process is repeated iteratively until selected stop conditions are met. These stop conditions can be a certain χ^2 error level, a certain amount of iteration steps, or if the difference between two consecutive models is below a certain threshold. The inversion results can be visualized directly in pyGIMLi or together with the results from ERT using PYTHON scripts developed at TU Wien. The combined usage of ptseis and pyGIMLi enables a PYTHON-only approach to process an SRT data set.

4 Assessment of the turn-off ramp of TEM soundings

4.1 Introduction

The aim of this case-study is to improve the understanding of signals transmitted and received by the TEM-fast system to gain an insight into the shape and length of the turn-off ramp. This information is important to improve the processing of TEM-data and ultimately the models obtained via inversion, with a focus on near-surface applications.

4.1.1 Background and motivation

The transient electromagnetic method was historically developed for deep ore investigations up to a few hundreds of meters. Therefore, the resolution of the uppermost part of the subsurface is rather low compared to other geophysical methods such as EMI and ERT. One reason for this lack of near surface resolution is the influence of the turn-off ramp of the pulse, which is used to create the primary electrical field. Although the TEM-fast system records data from as early as $4 \mu s$ after the current pulse is switched off, most of these earliest data points have to be removed during processing. This leads to a significant loss in resolution within the first couple of meters as well as to uncertainty, which data points should be included into the inversion process. These issues can be solved by quantification of the turn-off ramp (time) and correction of the TEM sounding curves, using the correct ramp times, within the inversion software.

Additionally to the aforementioned points, the influence of the turn-off ramp is also dependent on the near-surface resistivity distribution. To investigate this effect of the turn-off ramp on the measured signal (abbreviated to: ramp-effect) an experiment using different subsurface situations and ramp-times was done. The results of this experiment can be found in subsection 4.1.3.

4.1.2 Objective

The main objective of this case study is to quantify the turn-off ramp (time) of the TEM-fast system for various measurement setups (e.g loop sizes and system settings). This objective should be achieved by measuring the signals within the transmitter loop using an oscilloscope while the TEM-fast system is operating. Additionally, the measured turn-off times should be used to show the influence of the turn-off ramp on the inversion results.

4.1.3 Forward modeling to emphasize the importance

The ramp-effect can be visualized by forward modeling of the measured voltages within the receiver loop after the primary field is switched off. The forward modeling was done using a commercial software “ZondTEM” (Alex Kaminsky 2001), which was also used for data processing. To investigate this, a set of five turn-off ramps has been tested for three different subsurface situations. The turn-off time was chosen from a set of five different values:

1. 0.0 μs ; representing an immediate drop of the current pulse.
2. 2.0 μs ;
3. 4.0 μs ;
4. 6.0 μs ;
5. 8.0 μs ;

Each of those turn-off times has an individual color code, ranging in a 5-color spectrum from blue (0.0 μs) to red (8.0 μs). The subsurface situation was chosen from three different homogeneous models with increasing resistivity:

1. 10 Ωm ; representing a low resistivity case
2. 100 Ωm ; representing an intermediate resistivity case
3. 10000 Ωm ; representing a high resistivity case

All forward modeling results were obtained using the same 25 m loop (100 m cable) for transmitting and receiving of the transient signals (coincident loop setup). The signal was modeled using a current amplitude of 4 A.

The results can be found in figures 4.1, 4.2 and 4.3. All results are presented in terms of the measured signal (top subplot) and apparent resistivity (bottom subplot), which was calculated using a late time approximation directly within the ZondTEM application (Alex Kaminsky 2001). The results show, that an increase in subsurface resistivity leads to an increase of discrepancies between the curves from different ramp times. Additionally, the discrepancies are larger for longer ramp times. Therefore, the ramp-effect is more pronounced for longer ramp times and for higher resistivity of the subsurface. This influence is also described in the work from Fitterman and Anderson 1987.

4.2 Methodology and measurements

4.2.1 Basic measurement concept and signal structure

A conceptual model of two consecutive pulses (Transients) can be found in section 2.1.1 within figure 2.2. According to Christiansen, Auken, and Sørensen 2006, p. 189 a typical sounding consists of 1000 up to 10000 individual pulses, which are further processed

Ramp influence for 10 Ωm halfspace

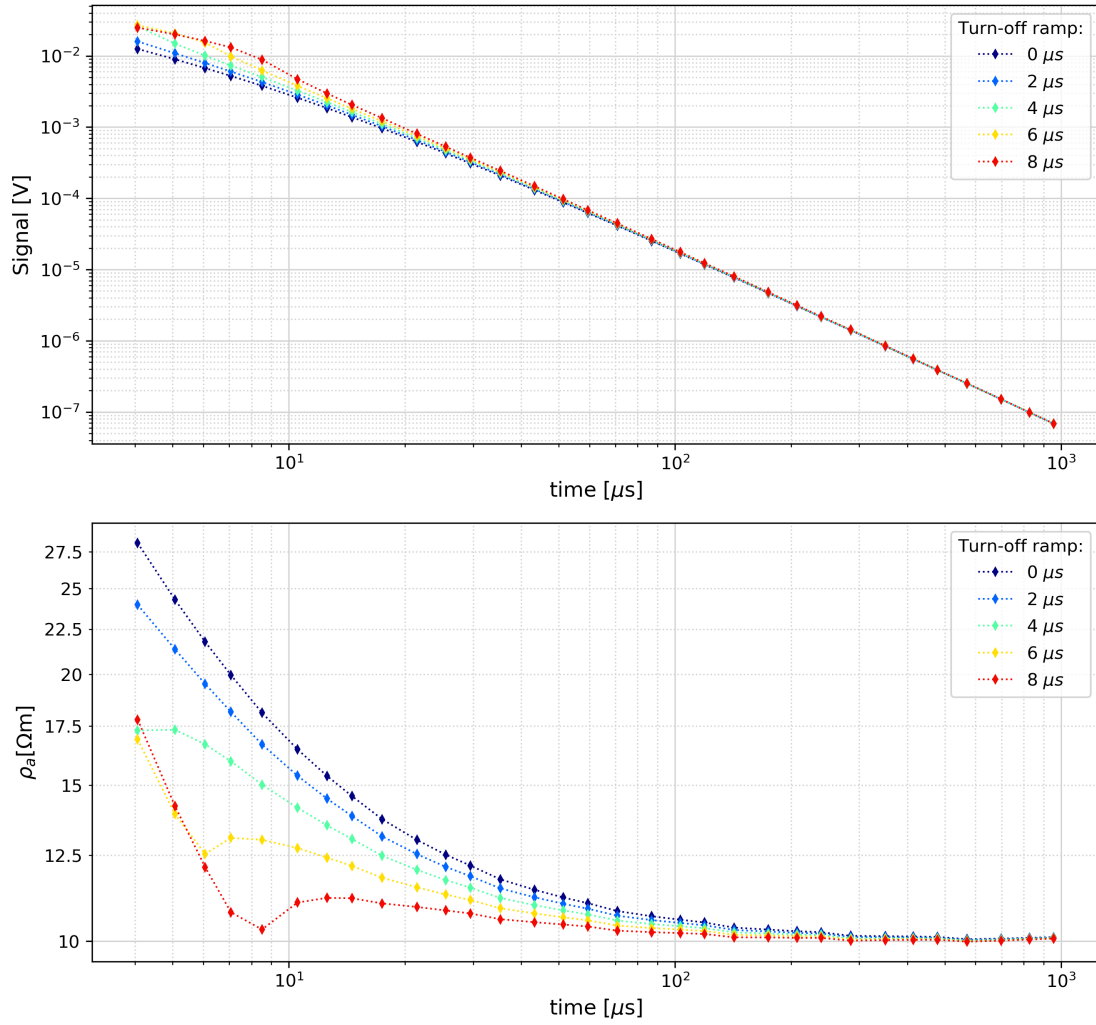


Figure 4.1: Forward modeling results calculated with ZondTEM software for a homogeneous 10 Ωm model.

Ramp influence for 100 Ωm halfspace

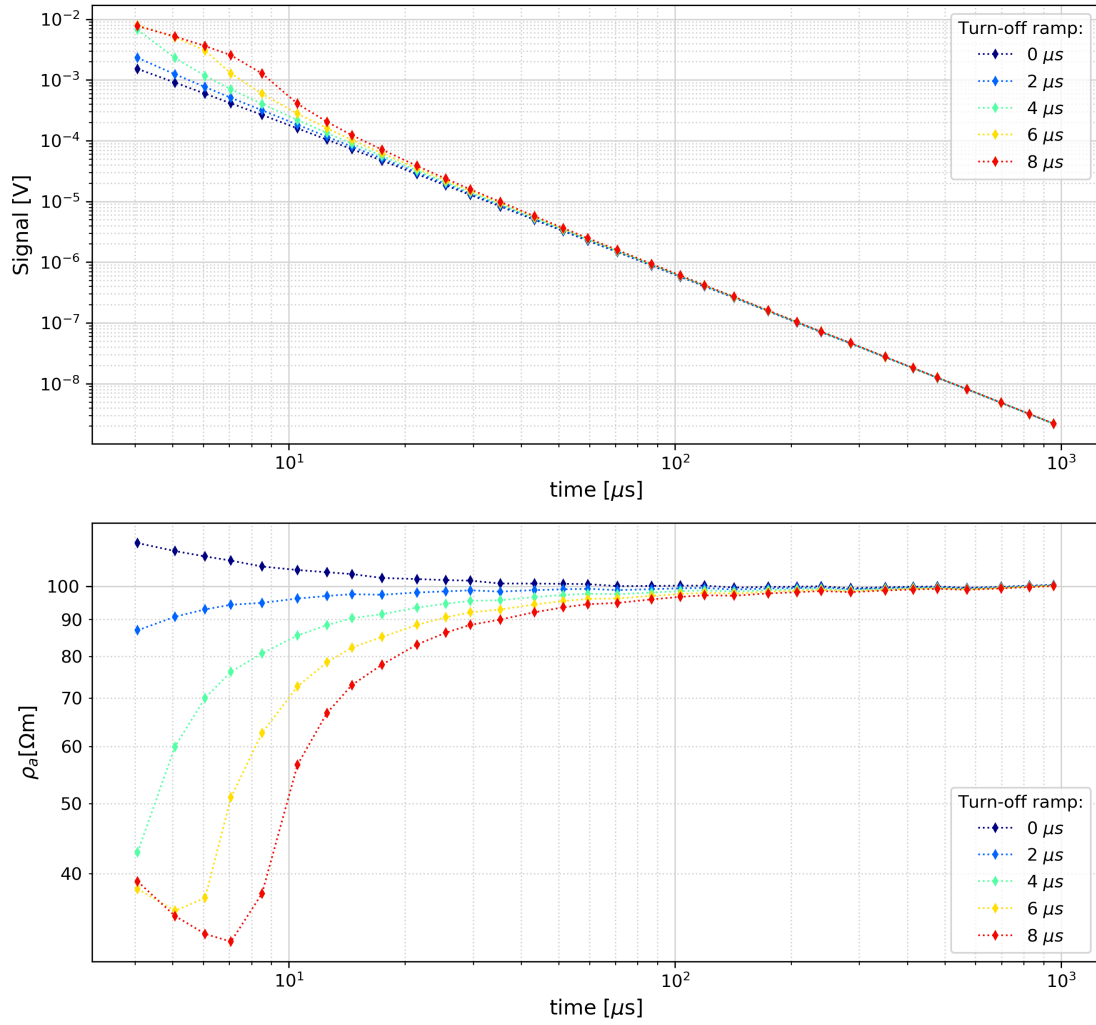


Figure 4.2: Forward modeling results calculated with ZondTEM software for a homogeneous 100 Ωm model.

Ramp influence for 10000 Ωm halfspace

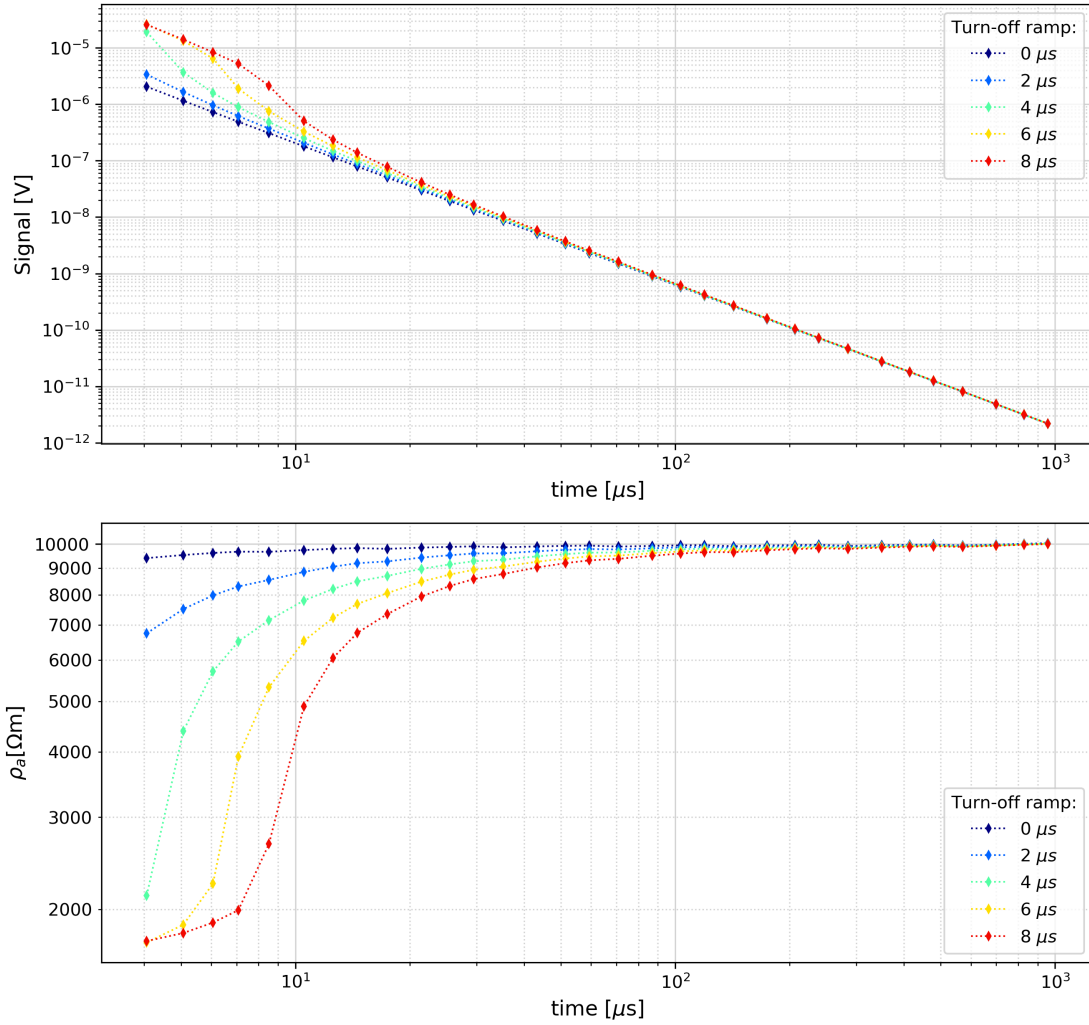


Figure 4.3: Forward modeling results calculated with ZondTEM software for a homogeneous 10000 Ωm model.

to increase the signal to noise ratio. Each of those individual pulses (Transients) is ended by the same turn-off ramp. To visualize one of the turn-off ramps within the full sounding signal it is necessary to choose adequate oscilloscope settings, as described below (refsubsec:osciMeas). To select adequate oscilloscope settings, it is necessary to gain a general understanding of the signal structure. This was done by following these steps using ever narrower time frames:

1. Visualization of a full measurement cycle, which is also called a sounding (Single stack see figure 4.6). Approximately 30 s of recording with a time division of 500 ms and a voltage division of 1 V.
2. Visualization of a single burst (figure 4.7). Approximately 35 ms of recording with a time division of 5 ms and a voltage division of 500 mV.
3. Visualization of a single transient pulse (figure 4.8). Approximately 50 μ s of recording.

4.2.2 Oscilloscope measurements

Table 4.1: An overview on how the Time-Key is affecting the timing and signal structure of the transmitted pulses. Adapted from the TEM-fast manual, by using a 3:1 ratio on the Ton+Toff time.

Time-Key	MaxTime [ms]	Active gates	on Time [ms]	off Time [ms]	Ton+Toff [ms]
1	0.064	16	0.23	0.08	0.31
2	0.128	20	0.47	0.16	0.63
3	0.256	24	0.94	0.31	1.25
4	0.512	28	1.88	0.63	2.50
5	1.024	32	3.75	1.25	5.00
6	2.048	36	7.50	2.50	10.00
7	4.096	40	22.50	7.50	30.00
8	8.192	44	37.50	12.50	50.00
9	16.384	48	67.50	22.50	90.00

The TEM-FAST signal processes happen in a time range of a few μ s up to a couple of ms. Table 4.1 gives an overview of the time ranges and how they are controlled by the Time-Key setting of the TEM system. The pulse lengths (alternatively On-Time) range from 0.23 to 67.5 ms, while the breaks between pulses (alternatively Off-Time, where voltage measurements are obtained) range from 0.08 to 22.5 ms. The first data point is always measured at 4 μ s and after that up to 48 data points are measured. Measurements with a multimeter do not have sufficient sample rates and are not able to store enough data points, to visualize the signal adequately. Therefore, an oscilloscope “Voltcraft - DSO 1084F”, was used which is capable of sampling down to a nanosecond while recording up to 64000 data points. Hence, a maximum record length of 64 μ s is possible, which is not enough to record a full duty cycle (On-Time + Off-Time) of minimal 310

μs (increases up to 90 ms for a Time-Key of 9). The sample rate can be decreased to increase the maximum record length. However, the sample rate shouldn't be decreased arbitrarily because this might lead to an under-sampling of the signal. Therefore, the adequate selection of the sample rate is critical. The sample rate is controlled by the size of the time division (horizontal axis) of the oscilloscope monitor. Furthermore, the size of the voltage division (vertical axis) is also critical for visualizing the signal amplitude. An exemplary picture of the oscilloscope screen, which emphasizes the meaning of those divisions can be found in figure 4.4. After finding an adequate setting (time and voltage division) to locate a single burst, it was necessary to set the trigger (controls the start of the signal display) to the point where the current pulse is switched off. The trigger was set to a point where the signal amplitude crosses a chosen amplitude level (trigger level). This point has to be selected according to the selected voltage division and has to be adjusted if the voltage division is changed.

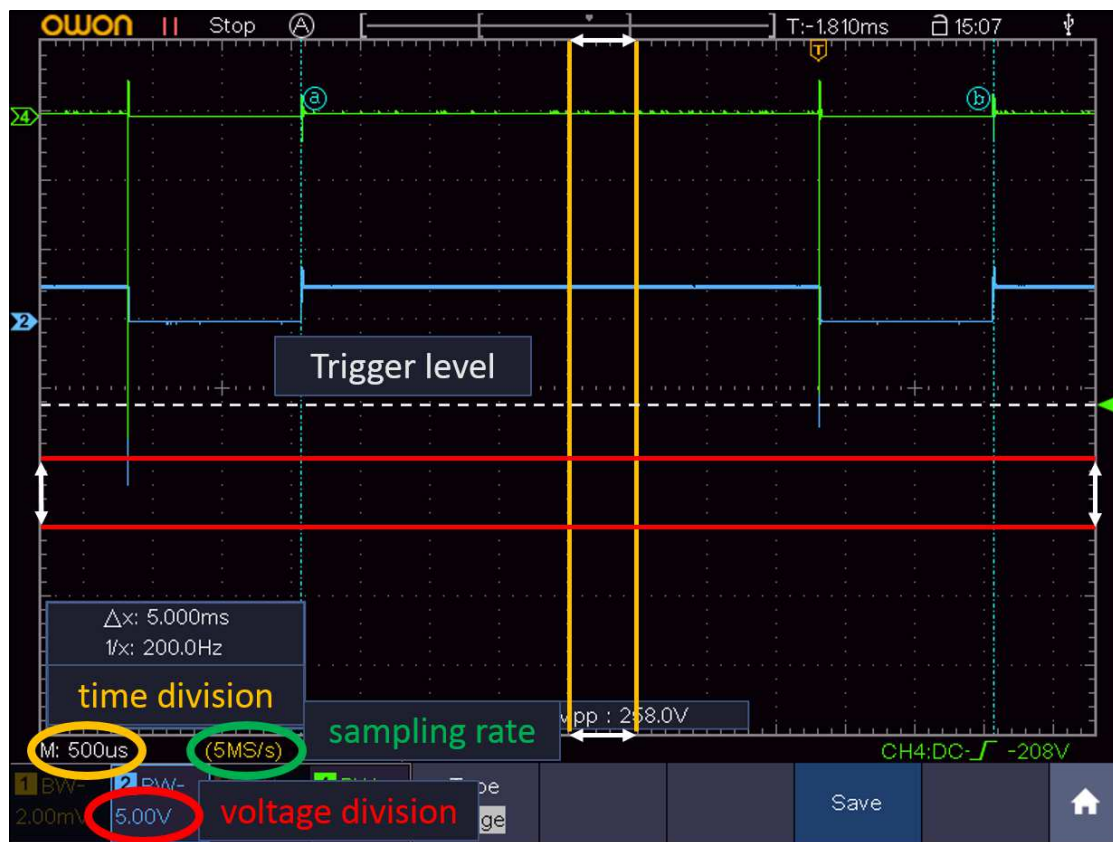


Figure 4.4: Time division in horizontal direction; voltage division in vertical direction and the trigger level is indicated by the gray dashed line. The picture in the background is from another oscilloscope, which is able to save screenshots - courtesy of Anton Lettenbichler.

To visualize the transmitted transient pulses, as well as the turn-off ramp, it is

necessary to conduct measurements of the current within the loop of the TEM system. The “Voltcraft - DSO 1084F” oscilloscope is not capable of directly measuring the current within a circuit. According to personal communication with Anton Lettenbichler (Geosono - e.U.) one way to directly measure the current, is the application of a so-called current probe. However, such probes are quite expensive and another option to obtain the current within a circuit is to use a shunt resistor. If the resistance (R) of the shunt resistor is known, it is possible to calculate the current (I) by measuring the voltage drop (V) at the resistor and applying Ohm’s law ($I = V/R$). This was done using Channel 1 of the oscilloscope (yellow). Channel 2 (light blue) was used to measure the voltage at the opposite end of the loop. The measurement setup can be seen in a circuit diagram in figure 4.5 and all measurements were done in field conditions. The measurements were repeated multiple times until adequate oscilloscope settings for each of the signal structure visualizations were found. Those measurements were stored on a usb drive and plotted using the matplotlib and numpy libraries of the open source PYTHON programming language.

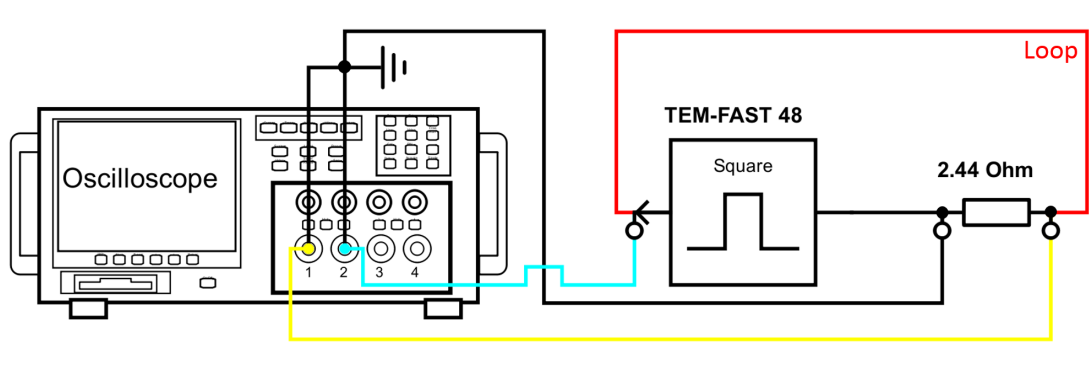


Figure 4.5: Circuit diagram of the oscilloscope measurements. (created using Scheme-it online tool from <https://www.digikey.at/schemeit/>)

4.3 Results

4.3.1 Signal structure

The TEM-fast system is capable of measuring multiple stacks during one data acquisition process. To gain a better understanding of the signal structure, figure 4.6 presents a single stack. This single stack consists of 17 bursts and stretches over a time of approximately 18 s. 13 of those 17 bursts are distributed equally along the middle of a stack, but 2 leading bursts and 2 trailing bursts are closer together and farther away from the bulk of the bursts. The author couldn’t find any information within the manual of the TEM-fast system on the reason for this distributions of the single bursts.

Subsequently, the next step is to visualize a single burst, which stretches over approximately 30 ms. Figure 4.7 shows only 45 of 63 total pulses to make the individual pulses

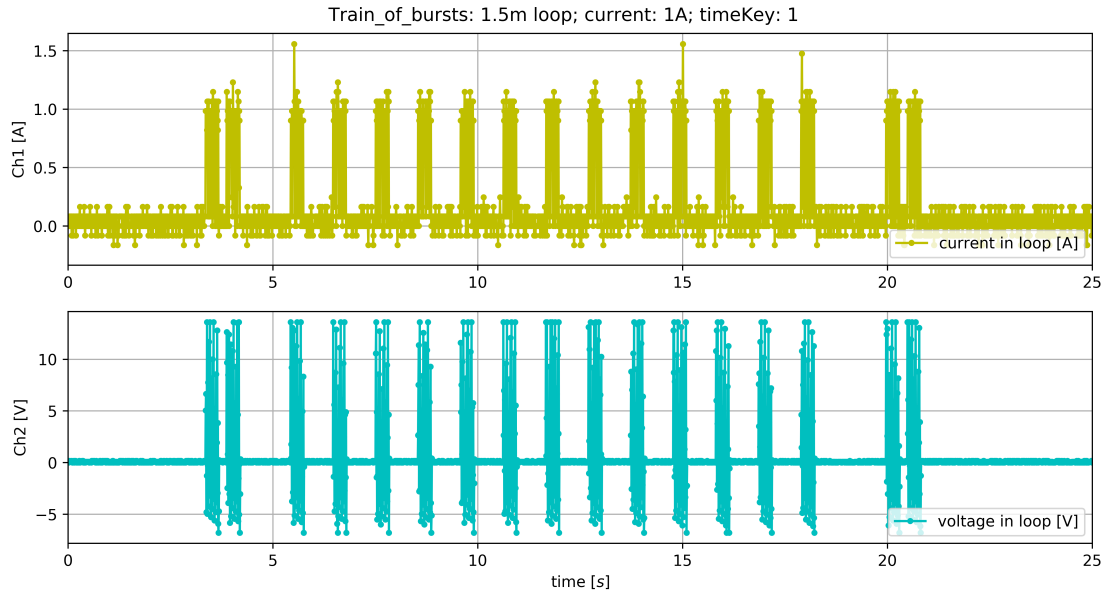


Figure 4.6: Full measurement cycle for a single stack of the TEM-fast system. It consists of a train of 17 bursts.

easier to distinguish from each other. Therefore, a single stack of one TEM-fast sounding consists already of 1071 (or 819 if you only count the 13 bursts in the middle of the signal train) individual pulses. Each of those pulses stretches, depending on the chosen Time-Key (see 4.1), from 0.23 ms up to 67.5 ms. All measurements to visualize the signal structure were done with a Time-Key 1 resulting in a pulse length of 0.23 ms. The shortest pulse length was chosen to decrease the maximum record length necessary for the visualization of the signal structure.

By zooming into figure 4.7 the shape of two successive pulses is revealed. The length of one of those pulses is exactly the same as the 0.23 ms expected from table 4.1 for a Time-Key 1 sounding. Unfortunately, the turn-off process is under sampled, since there is only one point at the beginning and the end of the ramp present. Therefore, the length of the turn-off ramp cannot be measured accurately.

Hence, the oscilloscope settings were adjusted again to zoom further to the exact moment in time where the current is turned off. Both channels show a high frequency oscillating behavior. According to personal communication with Anton Lettenbichler (Geosono e.U.), the oscilloscope Input-Capacitance and the loop-inductance are performing an LC-Oscillation at 25 MHz, damped by the 2.44 Ohm shunt-resistor. The resonance frequency of an LC-circuit can be described by formula 4.1:

$$f_0 = \frac{1}{2\pi\sqrt{LC}} \quad (4.1)$$

L represents an inductor with an inductance given in henrys and C a capacitor with the capacitance in farads. f_0 is the resonance frequency in Hz. This HF noise is suppressed

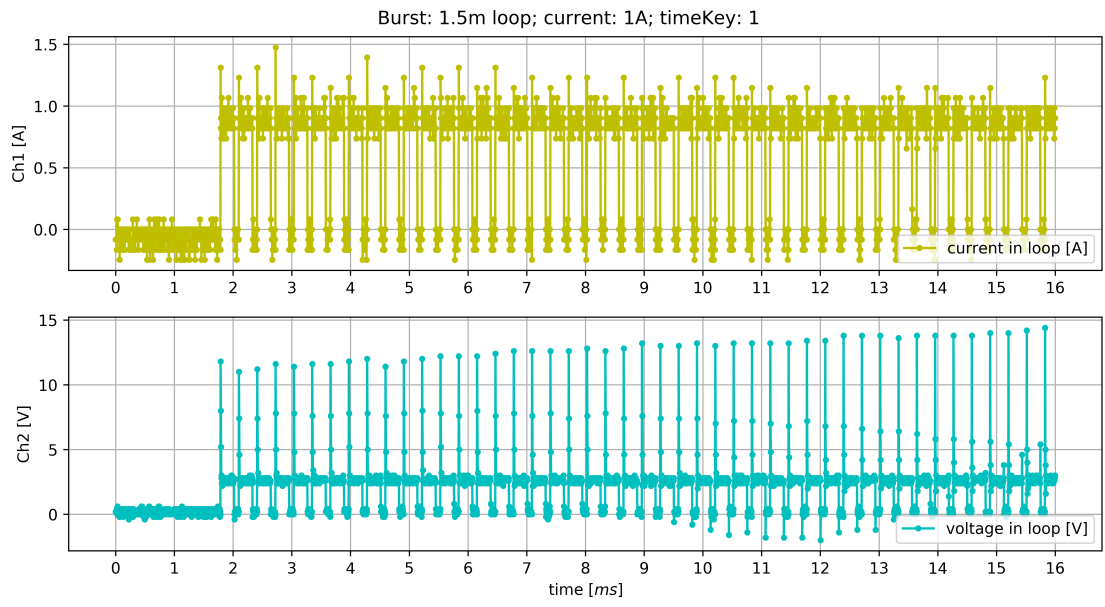


Figure 4.7: One of the 17 bursts of a stack. It consists of 63 single pulses.

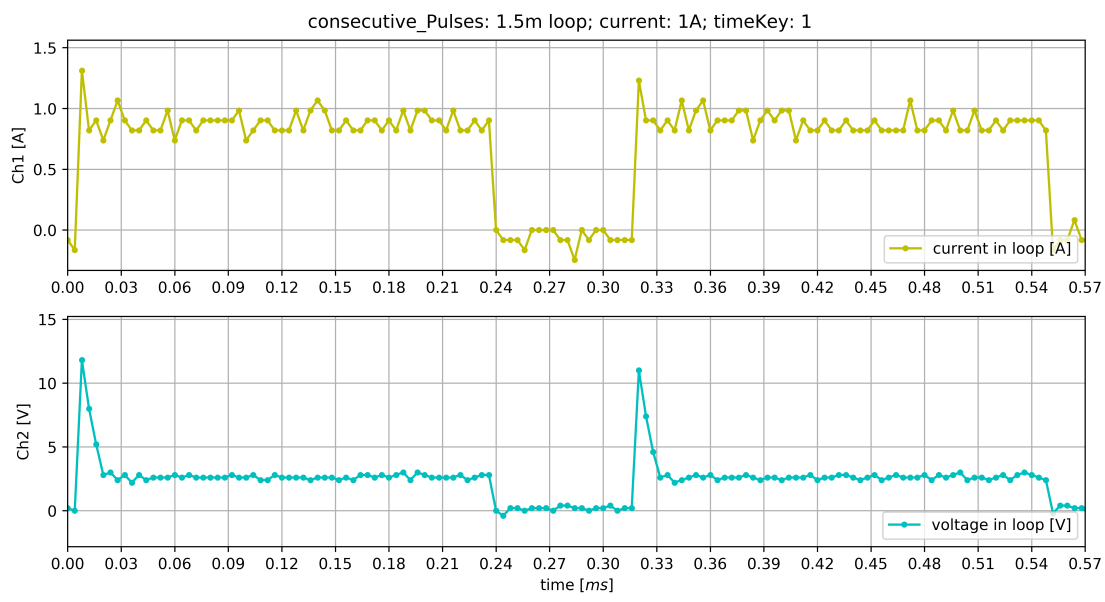


Figure 4.8: Two subsequent parts of two of the total 63 pulses.

at later measurements by using the signal averaging function of the oscilloscope, except in figure 4.15, that shows a 10 MHz oscillation due to the higher inductance of the 3.12 m loop.

The voltage, measured with Channel 2 in figure 4.9 (bottom subplot), peaks immediately after the current is cut off into a maximum with inverted polarity. After that, the voltage oscillates a couple of times until it decays completely. Hence, a smooth decay as seen in the upper part of figure 4.11 is not observed and the ramp time cannot be directly quantified.

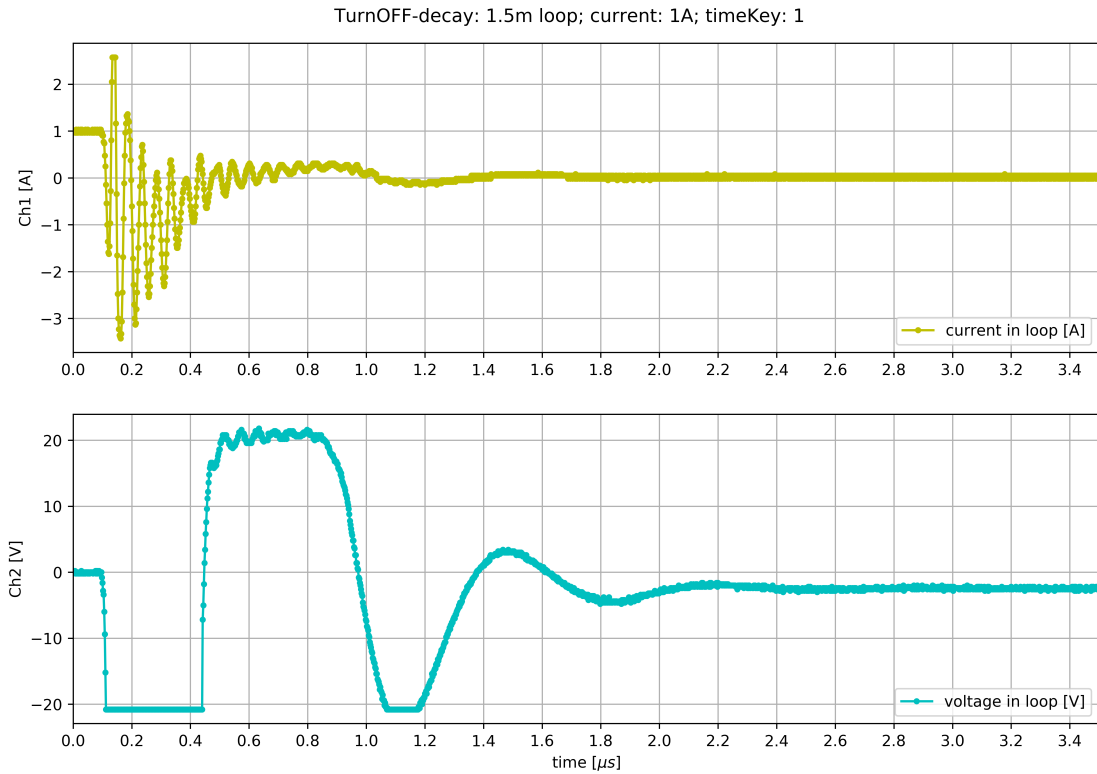


Figure 4.9: Zoom to the moment in time where the current is cut off. The voltage is limited to 20 V by the input stage of the oscilloscope.

4.3.2 Quantification of the length of the turn-off ramp

Although subsection 4.3.1 provides a comprehensive explanation of the signal structure, the question how to quantify the length of the turn off ramp remains unanswered. Figure 4.10 shows another plot of the voltage within the loop after the current is shot of. The voltage peak resembles the shape and reversed polarity (see figure 4.9) of the electromotive force as shown in the conceptual model in figure 4.11. Therefore, the first negative voltage peak, which is present right after the current is shut off (t_1), is related to the electromotive force caused by the current turn-off process. Moreover, figure 4.11 shows that the width

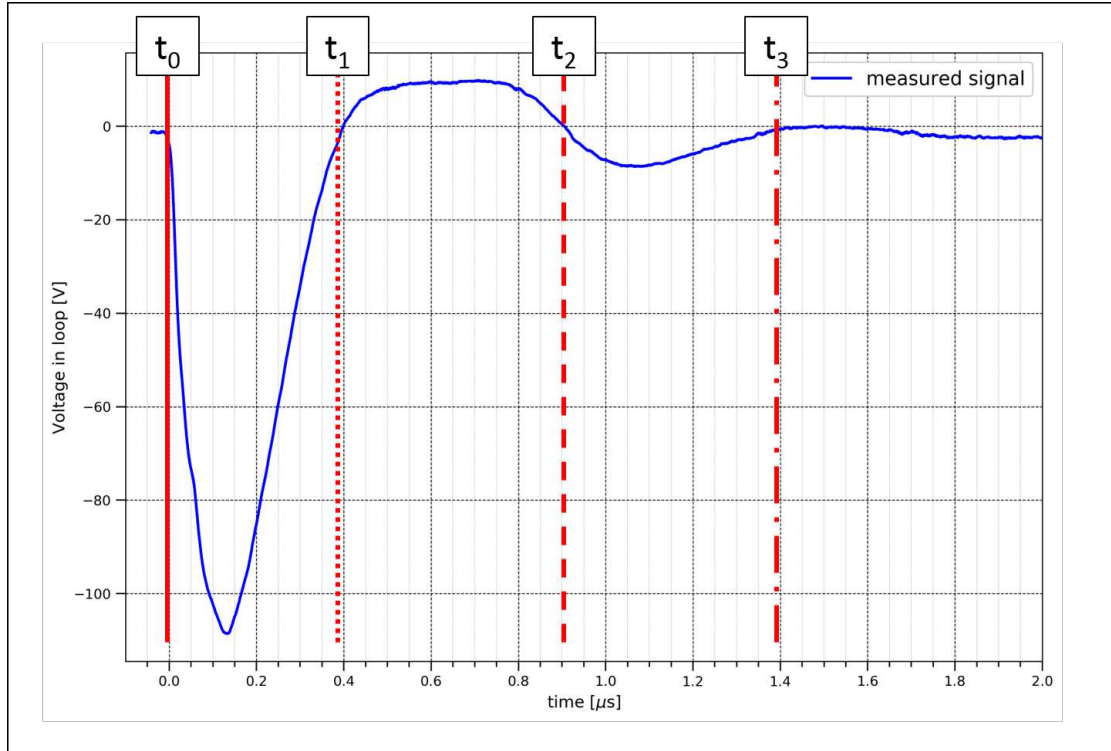


Figure 4.10: Voltage peak, after the current is shut off. The first red line (t_0) indicates the moment in time where the shut-off process is started. The other three red lines (t_1 , t_2 and t_3) mark the positions where the signal level drops back / crosses the initial signal level and represent possible turn-off times.

of the first voltage peak with inverted polarity has the same width as the turn-off ramp (indicated in the upper part of the plot). Hence, the width of the voltage peak was used to quantify the turn-off ramp (time). Therefore all subsequent measurements to quantify the length of the turn-off ramp of other TEM setups are only presented in terms of the voltage caused by the electromotive force.

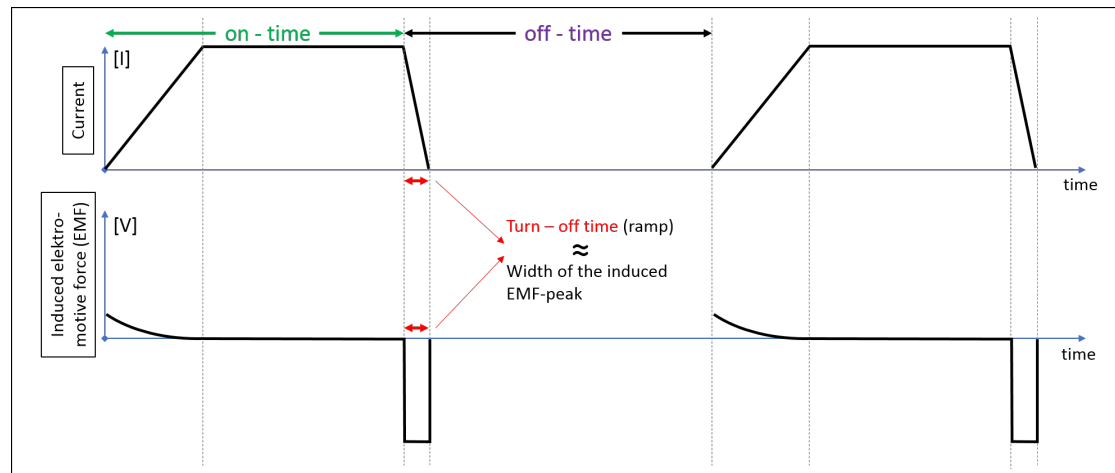


Figure 4.11: Conceptual model of two consecutive pulses adapted from Christiansen, Auken, and Sørensen 2006, p. 189 to emphasize the relation between the width of the voltage peak of the electromotive force and the turn-off time.

4.3.3 Results and discussion

To describe the influence from different parameters on the length of the turn-off ramp (time) four different comparisons were selected:

1. Comparison at two different sites: High and Low subsurface resistivity. (1 A transmitter current, 25 m cable)
2. Comparison of two different loop sizes. (4 A transmitter current)
3. Comparison of two different transmitter current intensities. (12.5 m loop - 50 m cable)
4. Comparison of two different amount of loop turns. (1 A transmitter current, 25 m cable)

The first comparison is presented in figure 4.12 and shows that there is almost no influence of the subsurface resistivity on the length of the turn-off ramp. The second comparison is presented in figure 4.13 and shows that the turn-off ramp is longer for the bigger loop by approximately $0.5 \mu s$. The third comparison is presented in figure 4.14 and shows that the the turn-off ramp is longer for 4 A transmitter current by approximately $0.2 \mu s$. Finally, the forth comparison is presented in figure 4.15 and shows that the

turn-off ramp is longer if the transmitter cable is used in 4 turns by approximately 0.1 μs . Since the TEM-fast system uses the same loop for transmitting and receiving of the signals 4 turns mean 2 transmitter and 2 receiver turns, which results in halving of the side length of the loop.

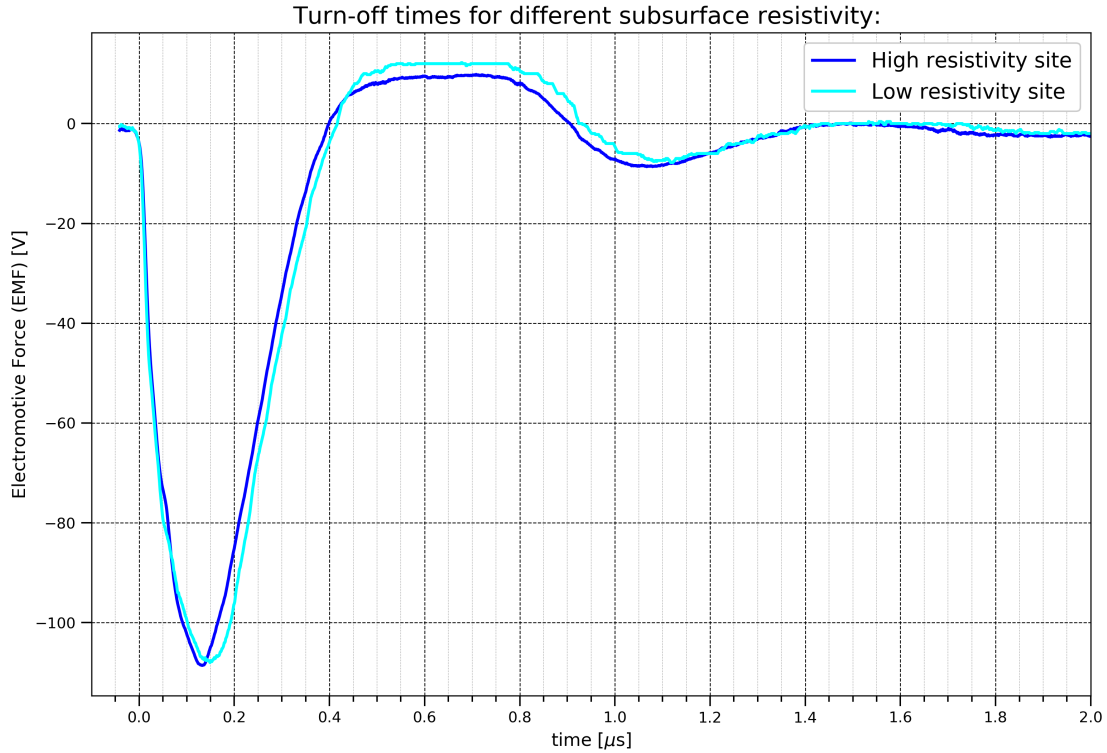


Figure 4.12: Comparison of two turn-off time measurements for a 6 m loop (25 m cable) at two different sites, with significant differences in subsurface electrical resistivity.

A table containing all measured turn-off times for multiple loop sizes and system settings can be found in 4.2. Those values can be used to adjust the turn-off time within the ZondTEM software, as described in 4.4. To summarize the findings it can be stated that an increase of the magnetic moment by higher transmitter currents, larger loops or more transmitter turns always results in a longer turn-off time.

4.4 Influence of the turn-off time on inversion results

Figure 4.16 shows the inversion results of an exemplary dataset, using a 25 m loop (100 m cable) and a current of 4 A. 8 different ramp times were chosen for this comparison. The inversion process was done using zondTEM commercial software as described in 3.2. The turn-off time (name in zondTEM to caption) and other pulse parameters can be set within zondTEM in the sub menu called "sounding settings"(see figure 4.17 for details of this sub menu). Initially the forward ramp parameter (name of the turn-off

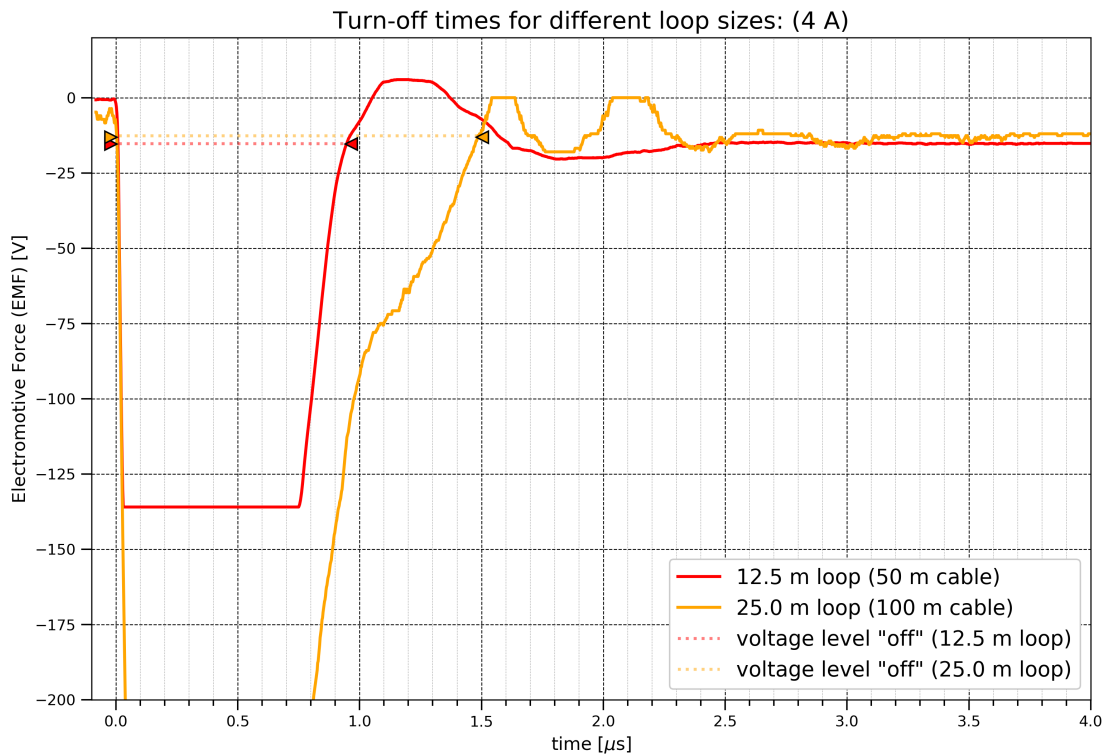


Figure 4.13: Comparison of two turn-off time measurements with two different loop sizes (12.5 m and 25 m) at 4 A.

Table 4.2: An overview of all measured turn-off times for multiple loop and system configurations.

id	cable [m]	side [m]	turns	current [A]	turn-off Time [μs]
1	6	1.5	1	1	0.15
2	6	1.5	1	4	0.17
3	12	3	1	1	0.23
4	12	1.5	4	1	0.27
5	25	6.25	1	1	0.40
6	25	6.25	1	4	0.45
7	25	3.125	4	1	0.50
8	25	3.125	4	4	0.55
9	50	12.5	1	1	0.75
10	50	12.5	1	4	0.95
11	50	6.25	4	1	1.05
12	100	25	1	1	1.30
13	100	25	1	4	1.50
14	100	12.5	4	1	2.10
15	100	12.5	4	4	2.50
16	400	100	1	4	10.00

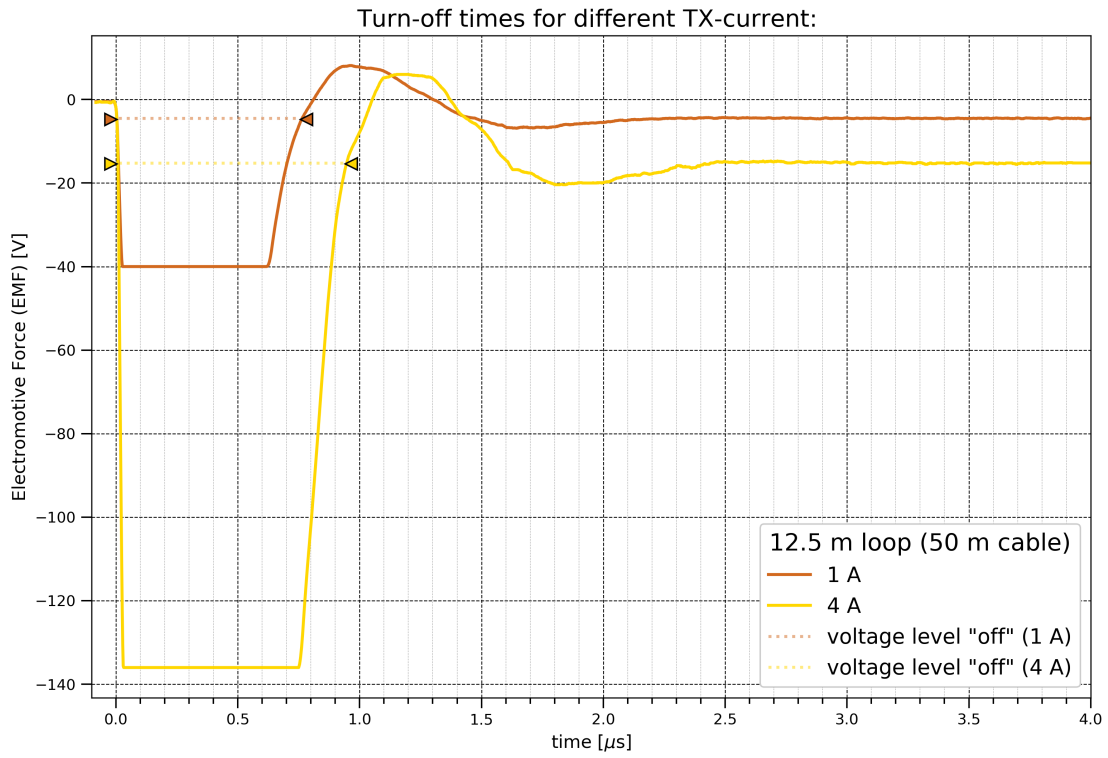


Figure 4.14: Comparison of two turn-off time measurements with two different current levels using a 12.5 m loop (50 m cable).

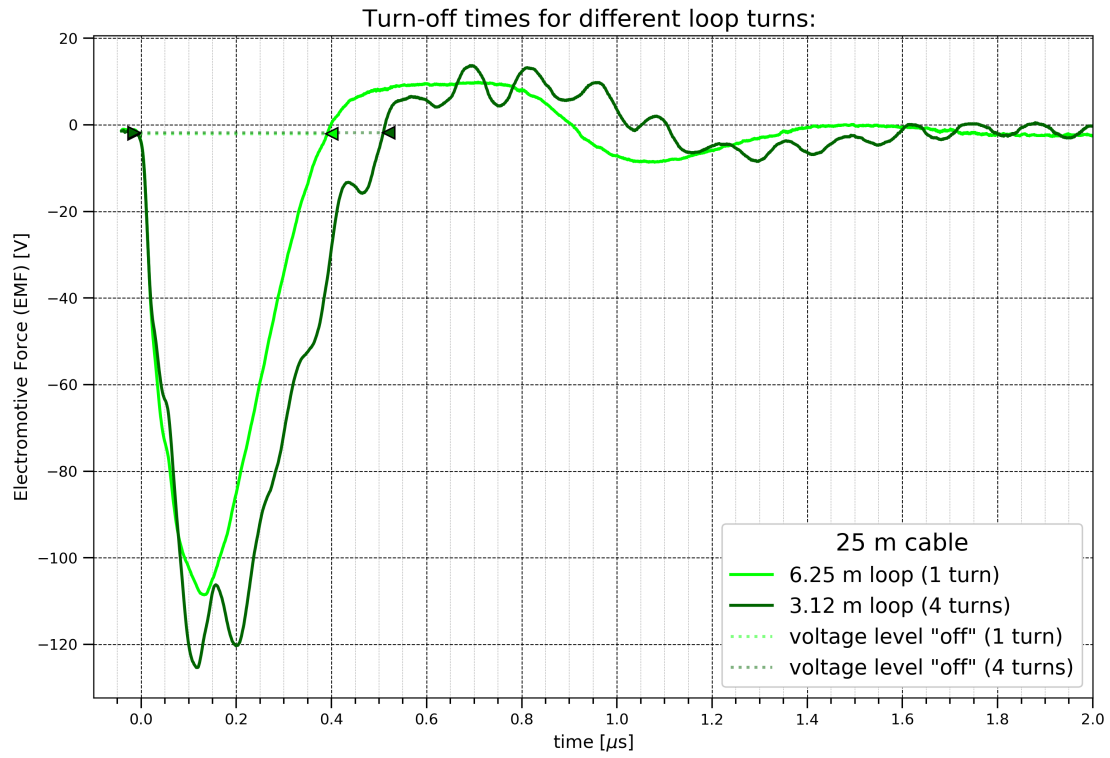


Figure 4.15: Comparison of two turn-off time measurements with a single turn (6 m side length) and 4 turns (3 m side length) using a 25 m cable.

time within ZondTEM) is set to $4 \mu\text{s}$ for a 25 m loop (100 m cable). The value of $4 \mu\text{s}$ is taken from the header of the sounding (.tem file). This parameter is called “deff” (see figure 4.18 for a screenshot of a .tem file), but is interestingly not closer explained within the TEM-fast manual (reference). Therefore, the author is not sure of the credibility of this parameter as the correct turn-off time. The comparison of the different ramp times reveals significant influence within the first 20 m (1/5 of the total depth of investigation) of the model. Especially, the reversed (high/low) resistivity and the depth to the first layer for a turn-off ramp greater than $3 \mu\text{s}$ is noticeable. After that all deeper layers show a similar increase to higher resistivity with depth.

Ramp influence on inversion result

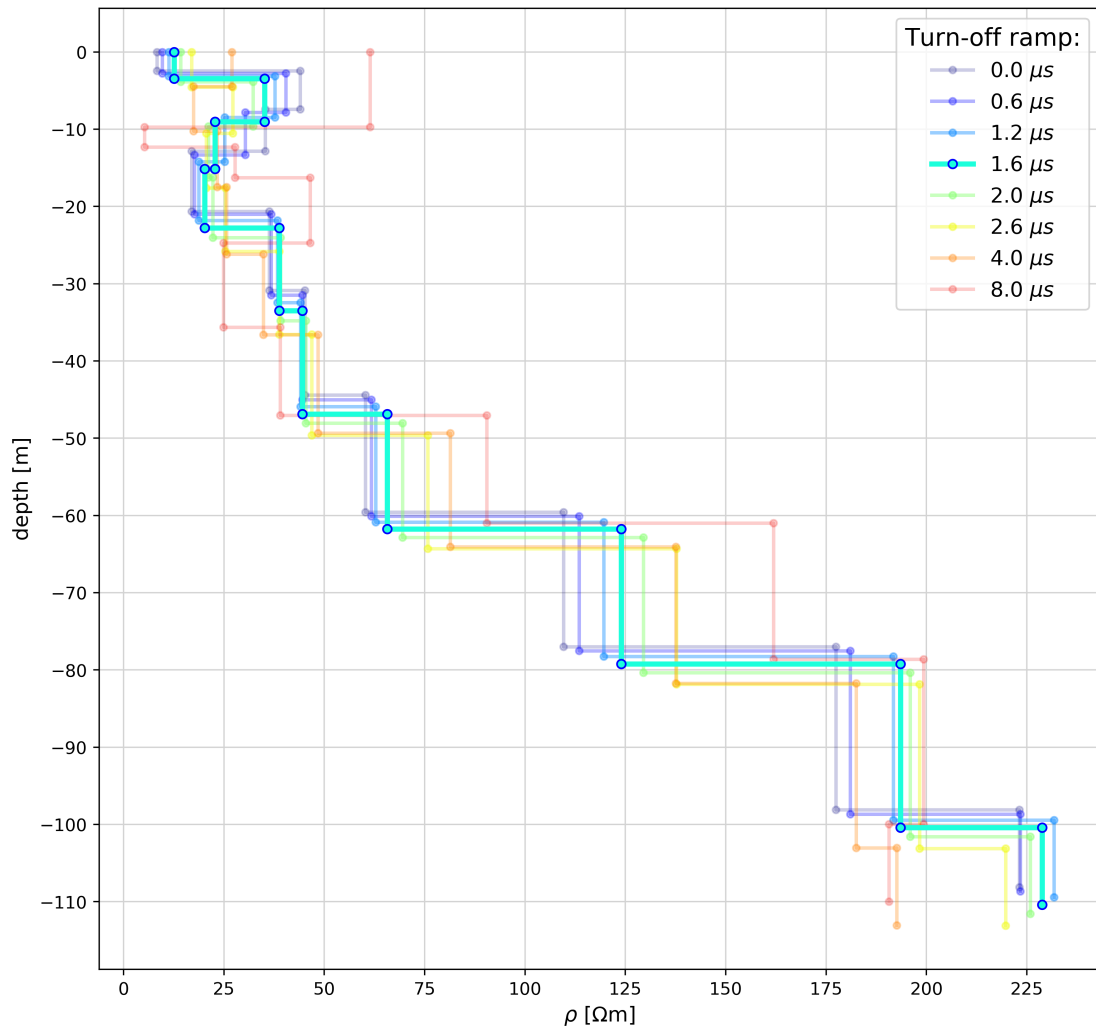


Figure 4.16: Changes in inversion results due to different turn-off ramp lengths. Inversions were calculated with ZondTEM for an exemplary data set measured with a 25 m loop and 4 A current.

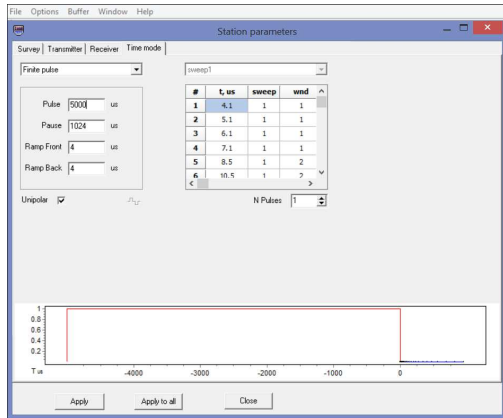


Figure 4.17: Sub-menu of the zondTEM software to control the TEM-pulse parameters.

```

1 TEM-FAST 48 HPC/52 Date: Mon Apr 16 09:35:31 2018
2 Place: KSELSBACH-BADNER-1
3 #Set m00001
4 Time-Range 5 Stacks 5 deff= 4 us I=4.2 A FILTR=50 Hz AMPLIFER=OFF
5 T-LOOP (m) 25.000 R-LOOP (m) 25.000 TURN= 1
6 Comments: 100 25
7 Location: x= +0.000 y= +0.000 z= +0.00
8 Channel Time E[I(V/A)] Err[V/A] Res[Ohm-m]
9 1 4.06 7.464e-001 1.256e-003 39.80
10 2 5.07 8.461e-001 1.090e-003 25.27
11 3 6.07 5.578e-001 6.797e-004 24.69
12 4 7.08 3.906e-001 4.752e-004 24.23
13 5 8.52 2.537e-001 3.100e-004 23.73
14 6 10.53 1.536e-001 1.835e-004 23.28
15 7 12.55 1.010e-001 1.191e-004 23.00
16 8 14.56 7.097e-002 8.454e-005 22.71
17 9 17.44 4.601e-002 5.442e-005 22.44
18 10 21.46 2.789e-002 3.267e-005 22.16
19 11 25.49 1.824e-002 2.136e-005 22.08
20 12 29.50 1.265e-002 1.510e-005 22.09
21 13 35.28 8.016e-003 9.730e-006 22.23
22 14 43.30 4.731e-003 5.767e-006 22.45
23 15 51.40 3.030e-003 4.372e-006 22.70
24 16 59.41 2.063e-003 3.036e-006 23.04
25 17 70.95 1.274e-003 1.725e-006 23.63
26 18 87.07 7.290e-004 1.109e-006 24.38
27 19 103.16 4.559e-004 9.464e-007 25.13
28 20 119.22 3.017e-004 8.923e-007 26.00
29 21 142.33 1.797e-004 5.178e-007 27.34
30 22 174.54 9.942e-005 6.246e-007 28.87
31 23 206.71 5.959e-005 6.160e-007 30.64
32 24 238.83 3.859e-005 6.044e-007 32.18
33 25 285.04 2.249e-005 1.867e-007 34.34
  
```

Figure 4.18: Header and some rows of data of a .tem data file. The parameter "deff" is set as the forward ramp parameter in zondTEM automatically.

4.5 Conclusion

This case study enhances the understanding of the signal structure of the TEM-fast system. Furthermore, it was possible to measure the turn-off ramp (time) of multiple different measurement setups. This information was used within the following case studies to correctly adjust the forward ramp in the ZondTEM inversion software. Additionally, the “ramp” case study also shows that the effect of the turn-off ramp on the measured signal is not the same for all subsurface resistivity. This ramp-effect is more pronounced, if the subsurface resistivity is increased, although the turn-off time remains mainly unaffected by an increase in subsurface resistivity. Although the measurements were repeated for different subsurface situation at different sites, the experiment should be extended to collect additional data sets at sites with an even higher subsurface resistivity, such as permafrost sites.

5 Investigation of a brick-clay resource using electromagnetic methods to quantify clay content

5.1 Introduction

This case-study is aiming to quantify the clay content within the subsurface using the transient electromagnetic (TEM) method. The TEM-method is, as described in 2.1.1, capable of mapping the electrical resistivity with depth. The electrical resistivity is a physical parameter that is dependent on the mineral type, the water saturation and the amount of clay in the subsurface. In general the TEM-method is applied at discrete measurement points, but it is also possible to measure adjacent points along a profile to generate a 2-D image of the subsurface by interpolation of the individual resulting 1-D models.

5.1.1 Background and Motivation

The raw material used to produce bricks consists of a mixture of fine-grain sediments, which contains a substantial part of clay minerals and is therefore commonly referred to as brick-clay. To quantify the amount of brick-clay in the subsurface and assess the profitability of a potential resource, geotechnical methods such as core drillings are commonly applied. Although they provide direct information at certain measurement points, their applicability is constrained by economic and logistical limitations. Furthermore, a simple interpolation of geotechnical data might lead to a wrong assessment of the subsurface situation, due to possible small-scale changes.

Clay minerals exhibit the strongest interfacial conduction and therefore lead to the highest bulk electrical conductivity (σ_0), which can also be expressed in terms of its inverse, the electrical resistivity (ρ , with $\rho = 1/\sigma$). Hence, geophysical methods sensitive to electrical resistivity (or conductivity) can map the clay content within the subsurface. In contrast to geotechnical methods, geophysical methods provide a continuous image of the subsurface. Extensive investigations to gain the same resolution using only geotechnical methods, would render site investigation prohibitable expensive.

5.1.2 Objective

To improve the understanding of electromagnetic signals and their resulting images the ERT method was used for validation. The transient electromagnetic method (TEM), which is mainly used to characterize deep structure, can be validated in a case study

which aims at the characterization of the first 40 m of the subsurface. Furthermore, the electromagnetic method at low induction number (EMI) was used to verify that there are no metallic objects present in the vicinity of the measurements.

5.1.3 Study area

The study area is located 3 km south of the Viennese border in Lower Austria, within the district of Mödling. Geologically the investigated site is situated within the Vienna basin, that consists typically of gravel-layers, followed by layers with varying sand- and clay content. Figure 5.1 shows an overview of the investigated site. The continuation of a clay layer to the south of the currently excavated brick-clay pit (GK M34: “Rechtswert”: 1287 m “Hochwert”: 329448 m) has to be validated to justify the extension of the excavation in this direction.

5.2 Field measurements

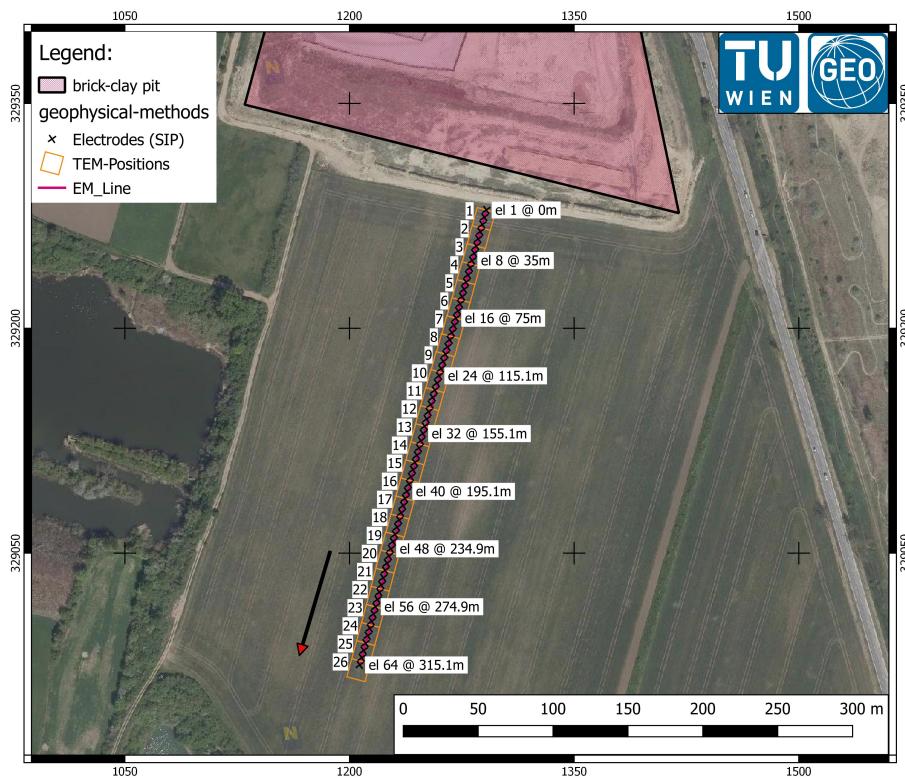


Figure 5.1: Overview of the study area, the purple area indicates the existing brick-clay pit, the orientation of the geophysical profiles is indicated by the black arrow.

All measurements have been conducted on the 10th of October in 2018 at dry ground conditions. The temperature was between 8°C in the morning and 22°C at noon. All

three geophysical methods were applied along a single profile for cross-validation of the different methods. The direction of measurements was roughly N-S as indicated by the arrow in Figure 5.1. Therefore, the beginning of each geophysical section is closest to the existing excavation site.

In total 26 TEM-soundings were obtained using a 50 m cable. The cable was extended in a 12.5 m by 12.5 m square on the ground and used for transmitting and receiving (coincident or single loop configuration) of the transient pulses. This (single loop) configuration is used to speed up the field work, since only a single cable has to be moved after each measurement. The measurements were done with a TEM-FAST 48 HPC system (AEMR, company) using 3 stacks and measurement time between 4 and 256 μs using 24 active gates for sampling of the received signal. This setup allows an approximate depth of investigation of 35 m.

EMI measurements were done along the same Profile indicated by the purple line in Figure 5.1 and were repeated in the other direction for validation purposes. The measurements were obtained using a CMD-Explorer (GF instruments, s.r.o.) in hi-Mode, which uses 3 different coil distances to obtain simultaneous measurements of electrical conductivity at 2.2 m, 4.2 m and 6.7 m depth.

ERT data was collected using the DAS 1, Electrical Impedance Tomography System (Multi Phase Technologies, LLC) using 64 stainless steel electrodes with a separation of 5 m between them. To improve data quality, shielded cables (coaxial) were used. Furthermore, the measurements were obtained using a dipole-dipole configuration (skip0 and skip3). This setup allows an approximate depth of investigation of 50 m. The measurements were obtained at 14 discrete frequencies between 0.1 Hz and 225 Hz, but to validate the findings from TEM measurements only the results at 1.0 Hz are presented.

Additionally a grain-size distribution analysis was performed by the company owning the brick-clay pit. The sample location was chosen at the outcrop of the clay pit closest to the start of the geophysical profile. Due to topography the first sample was taken 5 m below the surface at which the geophysical profile is situated. This offset was taken into account, when creating the clay content comparison in Figure 5.10. The complete results can be seen in table 5.1.

5.3 Transient electromagnetic data processing

Before inverting the TEM data it is necessary to assess the data quality and consistency (see section 3.2) of the measurements. This can be done by visualizing all measurements in a single plot for both the measured signal (5.2) and the apparent resistivity (5.3), while each individual sounding is represented by a color. This view can also be used to select a time-subset of the data set and remove unreliable sounding curves. In this case all of the sounding curves are similar and most of the data points between 7 and 110 μs have been used.

After completion of the inversion process of a TEM sounding it is obligatory to check how well the solved model is representing the measured data. Such a comparison is shown in Figure 5.4 and in this case, as well as in all other cases within this study the

Table 5.1: The grain size distribution at the outcrop closest to the start of the geophysical section.

sampleID	from [m]	to [m]	humidity relative [%]	sand > 63 μ [%]	silt + sand > 20 μ [%]	silt 2 – 20 μ [%]	clay < 2 μ [%]	silt & clay < 20 μ [%]
1	0.00	0.80	14.0	1.4	7.4	46.9	45.7	92.6
2	0.80	1.40	18.2	3.3	21.8	48.2	30.0	78.2
3	1.40	1.55	10.5	0.6	16.3	70.9	12.8	83.7
4	1.55	2.55	19.7	1.8	25.6	46.1	28.3	74.4
5	2.55	3.35	13.8	0.8	19.8	49.2	31.0	80.2
6	3.35	3.65	21.5	10.3	74.3	16.8	8.9	25.7
7	3.65	5.45	20.0	0.2	9.0	55.7	35.3	91.0
8	5.45	7.30	15.9	0.2	4.7	56.6	38.7	95.3
9	7.30	8.50	21.4	0.2	5.3	56.1	38.6	94.7
10	8.50	9.20	12.3	0.3	12.5	51.0	36.5	87.5
11	9.20	11.20	16.3	0.4	4.8	56.3	38.9	95.2
12	11.20	12.40	10.5	0.9	7.0	57.2	35.8	93.0
13	12.40	13.20	17.5	0.6	10.5	56.4	33.1	89.5
14	13.20	16.00	12.4	0.3	6.7	56.4	36.9	93.3
15	16.00	17.20	10.5	4.8	12.2	48.3	39.5	87.8
16	17.20	17.45	18.4	0.4	19.8	61.5	18.7	80.2
17	17.45	17.85	18.4	0.4	8.6	61.4	30.0	91.4
18	17.85	17.95	20.1	1.7	33.7	50.0	16.3	66.3
19	17.95	18.85	19.4	0.1	5.5	59.7	34.8	94.5
20	18.85	19.05	19.8	0.1	27.4	50.4	22.2	72.6
21	19.05	20.35	16.4	0.2	4.9	57.7	37.4	95.1
22	20.35	21.55	19.0	0.8	17.6	55.7	26.7	82.4
23	21.55	22.85	18.3	0.2	8.3	55.7	36.0	91.7
24	22.85	23.85	19.5	0.6	21.0	51.0	28.0	79.0

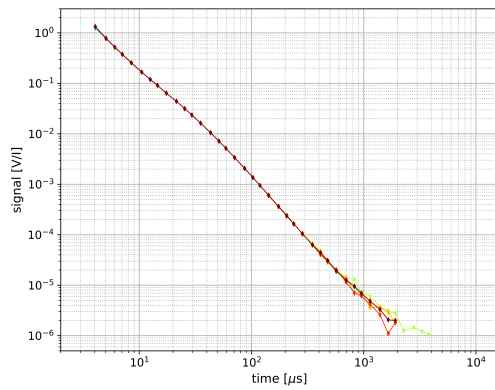


Figure 5.2: Representation of the full TEM data set in terms of the measured signal.

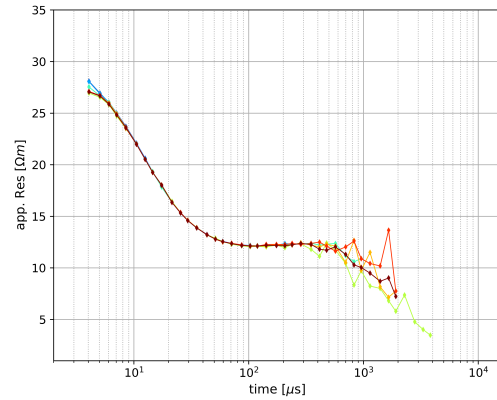


Figure 5.3: Representation of the full TEM data set in terms of the apparent resistivity.

model response is a good representation of the measured data.

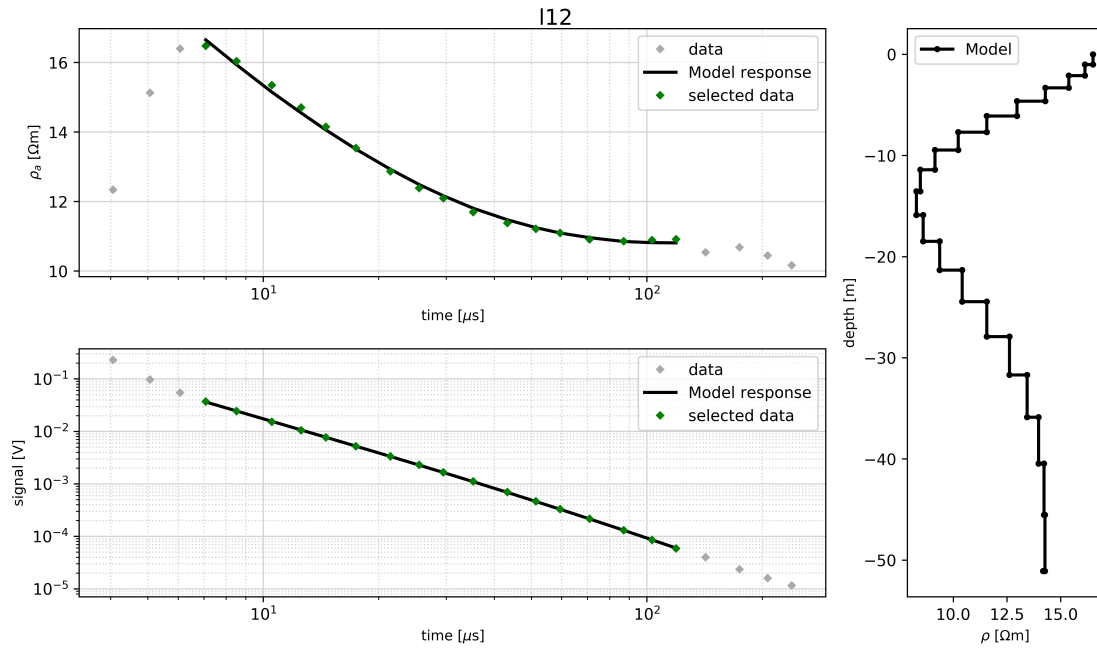


Figure 5.4: Raw data and forward modeling response of the resistivity/depth model on the right. The top left subplot shows the model response in terms of the apparent resistivity and the subplot below in terms of the measured secondary magnetic field.

5.4 Results and interpretation

5.4.1 Transient electromagnetics

Figure 5.5 shows a 2D section of all TEM-measurements. The 26 soundings were interpolated to get a continuous color-coded image of the subsurface resistivity distribution. The locations of the soundings are indicated by the black rectangles and the distance along the x-axis is chosen according to the ERT-profile distance (Figure 5.1). The position of the first sounding is offset by 6.25 concerning the first electrode of the ERT-profile. Red areas within the image indicate higher resistivity up to $25 \Omega m$, while the blue areas indicate lower resistivity down to $8 \Omega m$. This contrast can be interpreted as different lithological layers in the subsurface, which can be summarized by the following 4-layer model:

1. The uppermost layer, down to 5 m depth, can be related to a mixture of sand and gravels, which have typically higher resistivity than silts and especially clay sediments.
2. The second layer is a transition zone with decreasing electrical resistivity, that can be related to a silt/clay layer.
3. The third layer starts at approximately 12 m depth and consists of material with the lowest electrical resistivity. This layer can be related to the highest clay content within this subsurface section.
4. The fourth and bottom layer shows a significant increase in electrical resistivity, which can be related to a decrease in clay content.

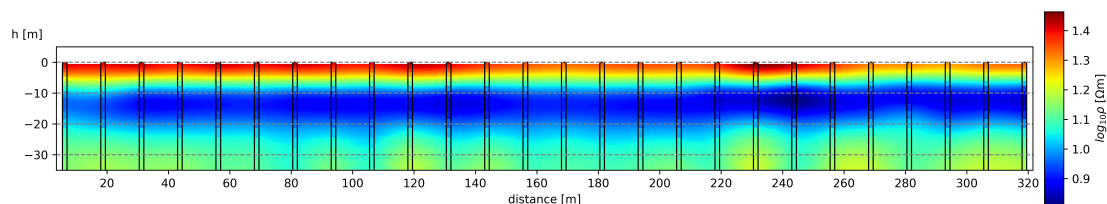


Figure 5.5: TEM section, starts at 6.25 m offset regarding the ERT-profile

5.4.2 Electromagnetic profiling

The out-of-phase part (blue curves) in Figure 5.6 shows the variation of electrical conductivity at three different depths (2.2 m, 4.2 m, 6.7 m) along the measurement line. The in-phase part (red curves) is a measure of data quality and can be used as an indicator of the presence of metallic structures in the subsurface. In this case both parts show smooth transitions along the profile. Especially the non-existence of peaks in the in-phase part is a strong evidence that there are no metallic structure in the vicinity of

the profile. To evaluate data quality the measurements were also obtained moving back in the other direction along the same profile (from South to North - Figure 5.1). Figure 5.7 shows both measurements plotted against each other to visualize their agreement. It can be observed that apart from some outliers most of the data points are reproducible when moving in the other direction along the same profile.

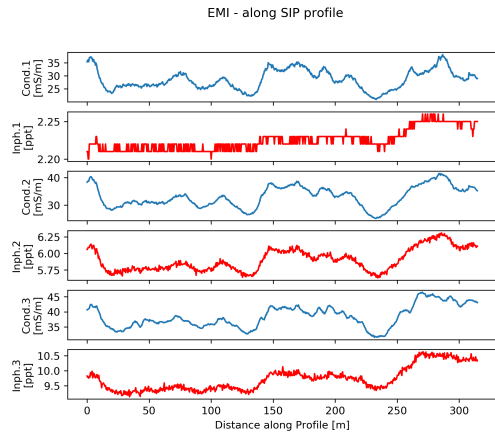


Figure 5.6: EMI measurement in terms of electrical conductivity [mS/m]; The blue curves show the electrical conductivity at 2.2 m, 4.2 m and 6.7 m (Cond1, 2 and 3); The red lines show the in-phase part, at the same depths.

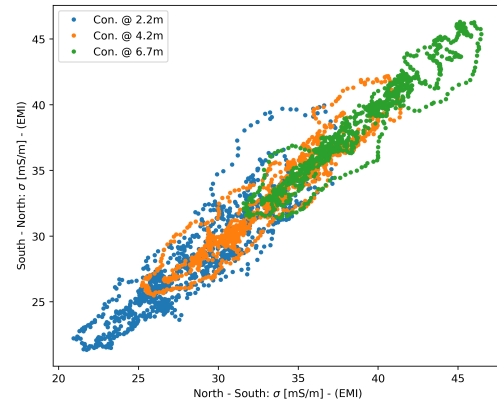


Figure 5.7: Comparison of EMI measurements obtained in two different directions along the profile for different coil separation resulting in 3 exploration depths.

5.4.3 Electrical resistivity tomography

The ERT results (Figure 5.8) are, like the TEM-section, shown in terms of electrical resistivity. Again, red areas represent higher resistivity while blue areas represent lower resistivity. The absolute values of the ERT image are lower than the values obtained by the TEM-soundings. The contrast between the layers shows similar features as the TEM-section (Figure 3). The lowest resistivity is also observed between approximately 12 m and 24 m depth and can be related to higher clay content than their surroundings. Like the TEM-section the ERT profile also shows the lowest resistivity from 210 m to 270 m within the low resistive layer. The subplots on the right side of Figure 5.8 show the direct comparison of electrical resistivity (as a 1-D log) at the position of the L12 - TEM sounding. The shape of the resistivity 1-D log fits almost perfectly to the TEM-sounding. The direct comparison(5.9) at two locations along the profile shows that both methods are in agreement with each other. But the agreement is significantly better in the latter part of the profile, which might be related to a reduced depth-resolution of the ERT method at the border of the profile. Furthermore it has to be noted, that the least resistive part of the logs is observed approximately 2 m closer to the subsurface in the

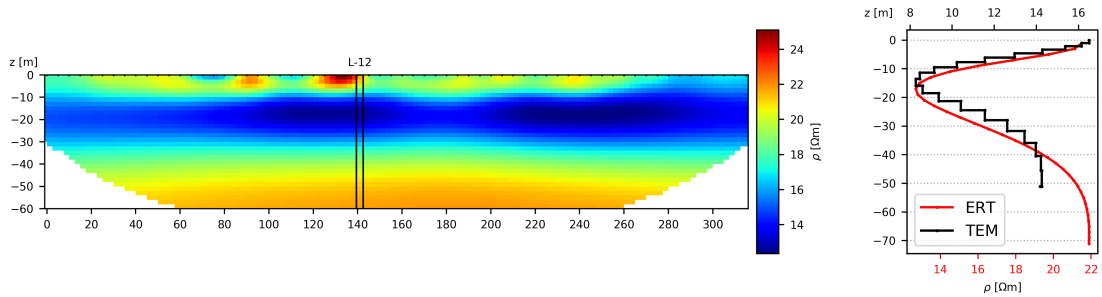


Figure 5.8: ERT-section at 1.0 Hz; the subplot on the right side show the comparison to the TEM measurement at this position.

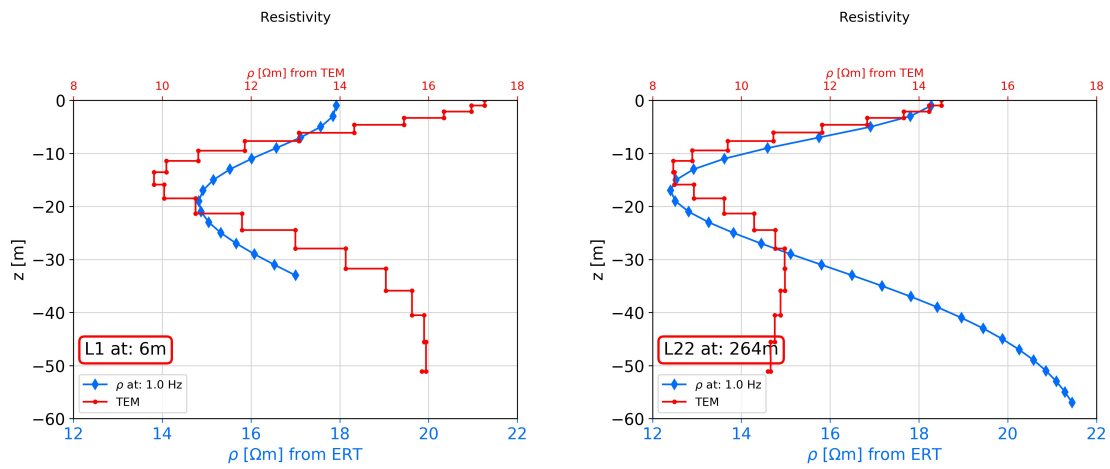


Figure 5.9: Direct comparison of the resistivity 1D-log obtained by the TEM method and the ERT method at two different positions along the profile.

TEM model.

The additional results from the grain size distribution analysis are presented in terms of the clay content in Figure 5.10. Although the samples were obtained closer to the TEM sounding at the start of the profile, the additional comparison to a sounding in the middle of the TEM profile reveals a relative decrease in electrical resistivity. This decrease might be related to a further increase of clay content along the profile.

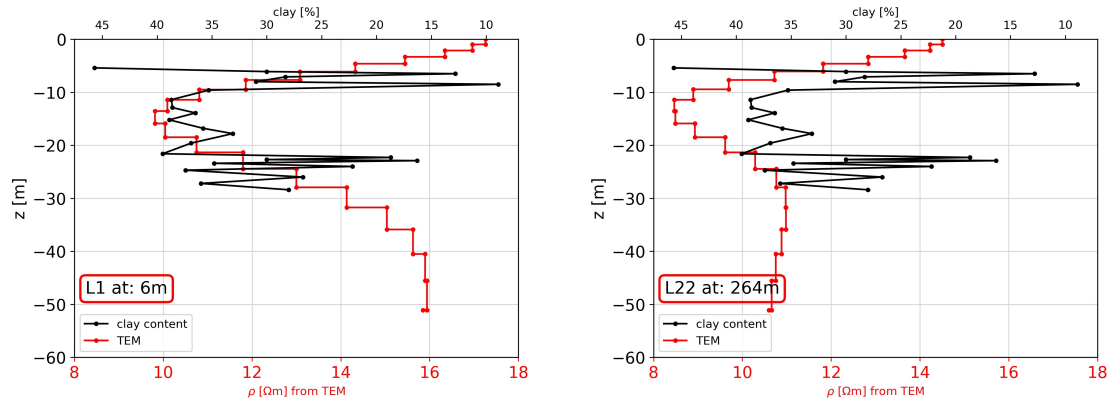


Figure 5.10: Direct comparison of the percentual clay content and the electrical resistivity from the TEM method.

5.5 Conclusion

This case study provides an opportunity to evaluate the capability of the TEM method to provide a reliable measure of the electrical resistivity. The direct comparison to an ERT measurement along the same profile is revealing consistent results. Furthermore, it is possible to estimate the relative change of clay content along this profile by comparing the findings of a grain size analysis at the beginning of the profile to the change of the electrical resistivity along the profile. Especially the low resistive layer between approximately 12 m and 25 m is confirmed by both the ERT method and the TEM method. The continuation of this layer with the highest clay content to the south of the existing brick-clay pit can be confirmed. This could be validated further in the future by performing some core drillings along the geophysical profile.

6 Characterization of a clayey landslide by integral application of multiple geophysical and geotechnical methods

6.1 Introduction

This case-study is aiming to develop a new methodology to characterize clayey landslides. In particular, the applicability of the transient electromagnetic (TEM) method is investigated. The additional information from TEM measurements is used to help with the interpretation of commonly used geophysical methods such as electrical resistivity tomography (ERT) and seismic refraction tomography (SRT). To delineate possible near-surface drainage systems additional low-induction number electromagnetic (EMI) measurements were obtained. Direct methods, such as core drillings, dynamic probing and trial pits are used to validate the geophysical results.

6.1.1 Background and Motivation

Landslides are natural hazards posing a threat to infrastructure and human life. Understanding the internal structure of a landslide is critical for managing the associated risks. Geotechnical methods are a common way to characterize the subsurface properties of interest (e.g., lithology, water content, plasticity, etc.), yet they only provide information at discrete measurement points. Economic and logistic limitations constrain the applicability of geotechnical measurements to gain information with the required spatial resolution. Furthermore, a simple interpolation of geotechnical data might bias the result, since subsurface properties can change even at a small scale. Geophysical methods provide quasi-continuous information about subsurface properties, yet the quantitative interpretation of such results requires complementary data.

6.1.2 Objectives

To characterize a landslide it is necessary to describe the subsurface lithology and hydrogeology, while also delineating potential sliding planes. The delineation of sliding planes is necessary to estimate the volume of potential sliding material and assess the associated risks in case of a sliding event. A sliding plane can be distinguished by a contrast in physical properties such as electrical resistivity and seismic velocity, as well as by changing soil properties obtained geotechnical measurements.

The main focus of this case study is to evaluate the applicability of the transient electromagnetic method for landslide characterization. This is done by comparing the

results to, in terms of landslide characterization, more commonly applied methods such as refraction seismic tomography and electrical resistivity tomography. Furthermore, several well-established geotechnical methods were used to provide ground truth regarding potential sliding planes.

6.1.3 Study area

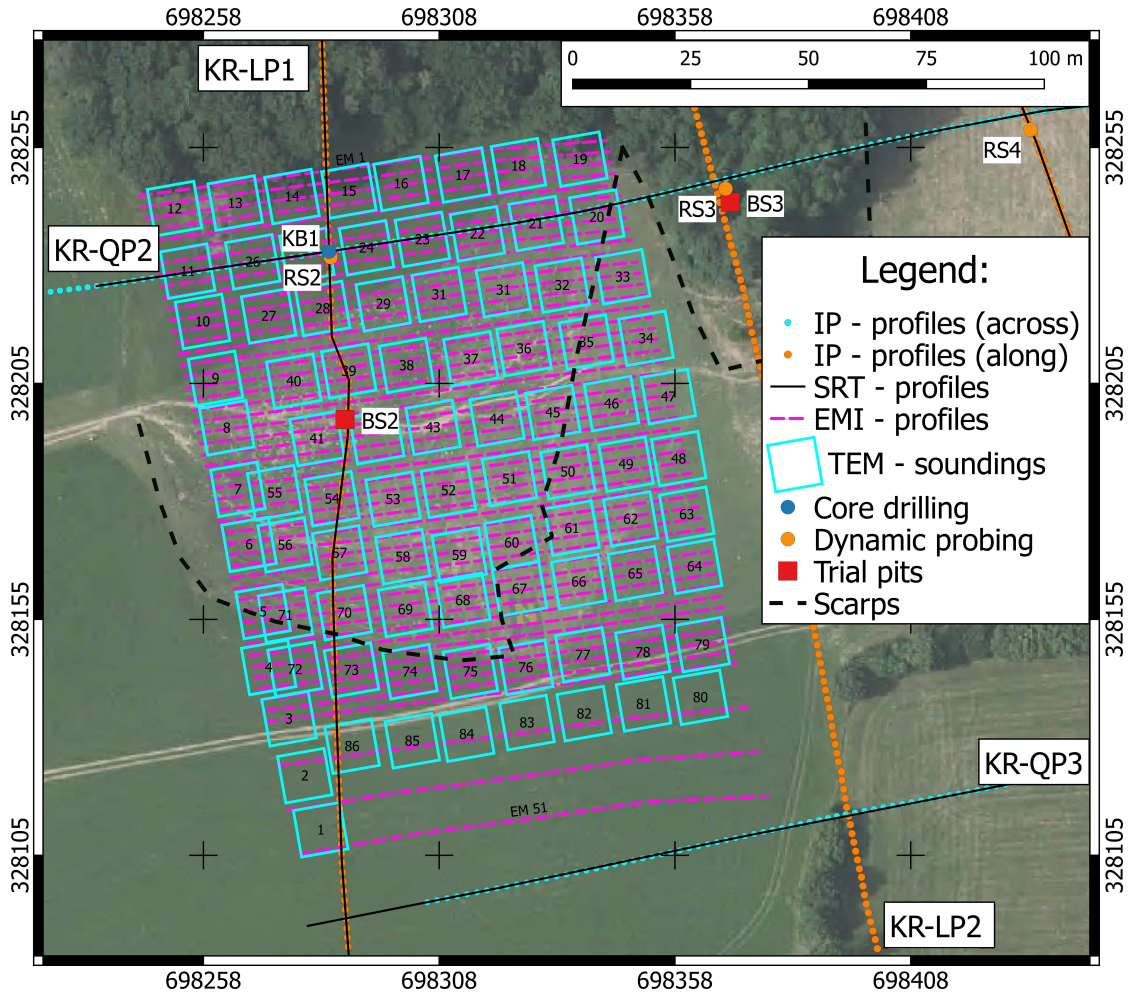


Figure 6.1: Overview of the Kreisbach study area. The border of the landslide is indicated by the black scarp line.

The study site is located in Lower Austria, within the district of St. Polten-Land close to the village of Kreisbach. Geologically the site is situated in the Flysch-Zone formation, consisting of interbedded strata of sandstone and claystone covered by a weathered clay layer. According to Schnabel et al. 2013 the investigated landslide is a complex rotational slide, which was known since 1996 and reactivated during heavy precipitation events in 2006. A geodetic monitoring network revealed a crouching of 1 cm/year up to 7 cm/year.

Figure 6.1 shows an overview of the south western part of the investigated site. The slope is crouching to the north of the map and poses a threat to a few houses and the creek called “Kreisbach”. A major landslide might not only damage the houses but may also clog the creek and potentially flood parts of the valley.

6.2 Field measurements

In total 86 TEM-soundings were obtained using a 50 m cable on the 16th of April in 2018. Those measurements are indicated by the cyan squares in Figure 6.1. The cable was extended in a 12.5 m square on the ground and used for transmitting and receiving (coincident or single loop configuration) of the transient pulses. This (single loop) configuration is used to speed up the field work, since only a single cable must be moved after each measurement. The measurements were done with a TEM-FAST 48 HPC system (AEMR, company) using 3 stacks and a measurement time from 4 μs to 256 μs at 24 active gates for sampling of the received signal. This setup allows an approximate depth of investigation of 35 m.

EMI measurements were done along 51 profiles separated by 2.5 m on the 16th of April in 2018 and are indicated by the purple lines in Figure 6.1. The measurements were obtained using a CMD-Explorer (GF instruments, s.r.o.) in hi-Mode, which uses 3 different coil distances to obtain simultaneous measurements of electrical conductivity at 2.2 m, 4.2 m and 6.7 m depth.

To map the entire landslide SRT data was collected along 5 profiles on the 2nd and 5th of October in 2017 at sunny and dry weather conditions. The measurements were obtained using a Summit Compact system and active 30 Hz geophones with a separation of 2 m. The profile lengths varied between 142 m and 352 m. A detailed view of the experimental setup in the south western part of the site can be seen in Figure 6.1. For validation of the TEM measurements only a single SRT-profile (QP2) will be presented in the results subsection 6.4.3.

ERT data was collected on 9th and 12th of October in 2017 using a Syscal Pro Switch 72 (IRIS instruments) with a separation of 2 m between the stainless-steel electrodes. A single measurement can utilize up to 72 stainless steel electrodes which leads to a profile length of 142 m with an approximate depth of investigation of 25 m. To cover the complete landslide, it was necessary to use the “roll-along” methodology, where the last 18 or 36 electrodes of the preceding measurement are re-used as the first ones for the next measurement. Re-using 18 electrodes will increase the covered profile by 106 m, while re-using 36 electrodes will increase the profile length by only 70 m. In total 6 profiles, with lengths varying between 142 m and 354 m, were measured on the 9th and 12th of October in 2017 at sunny and dry weather conditions. For this study only the profiles LP1 and QP2 were used, since those two crossed the area where electromagnetic measurements have been conducted (see Figure 6.1 for details).

To collect complementary ground truth data three different methods were applied between November 2017 and April 2018:

1. Dynamic Probing heavy (DPH) is an indirect method by which the rigidity of the

ground can be assessed. This is done by hammering a metal rod into the ground and measuring the penetration rate after each blow (blows are counted to progress 10cm of soil). Within this study 4 DPH were done, although only one is located in the area of interest.

2. Trial pits can be used to directly assess the first 5 - 6 m of the subsurface as well as to collect soil samples for later laboratory analysis. Within this study 4 trail pits were dug.
3. Core drillings can assess the subsurface and collect soil samples from greater depths depending on the budget. Due to logistical limitations only one such drilling was done at the intersection of LP1 and QP2.

The location of these geotechnical measurements are indicated in Figure 6.1. The samples collected from trial pits and the core drilling were analyzed to gather information on grain size distribution, water content, density and other geotechnical parameters.

6.3 Transient electromagnetic data processing

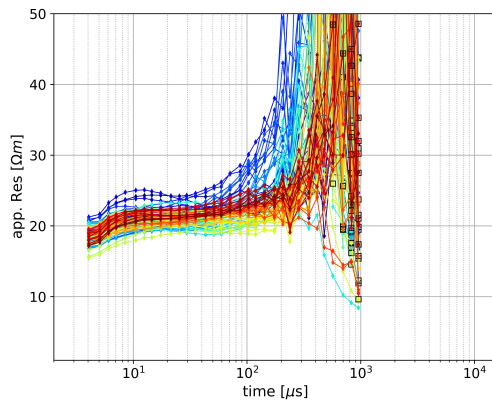


Figure 6.2: Representation of the full TEM data set in terms of the measured signal.

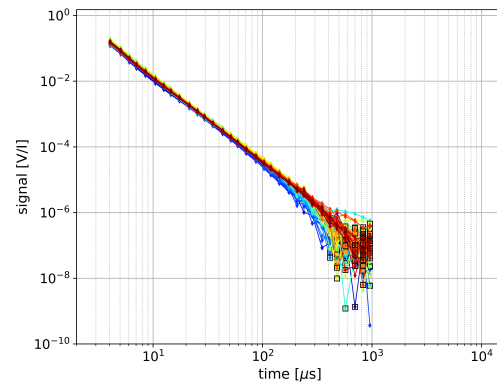


Figure 6.3: Representation of the full TEM data set in terms of the apparent resistivity.

The first step after data collection is to visualize the measured signal as well as the apparent resistivity calculated by the TEM-FAST device. This step gives an overview of the data quality and helps to decide which part of the signal can be used for inversion of the data. Such a first look of all 86 soundings can be seen in terms of the measured voltage and the apparent resistivity in 6.2 and 6.3 respectively. The measured voltage induced by the secondary magnetic field can be seen on the left and does not show any outliers until approximately 150 μs . The apparent resistivity on the right reveals more variability but most decay-curves are also smooth and do not show outliers until approximately 150 μs .

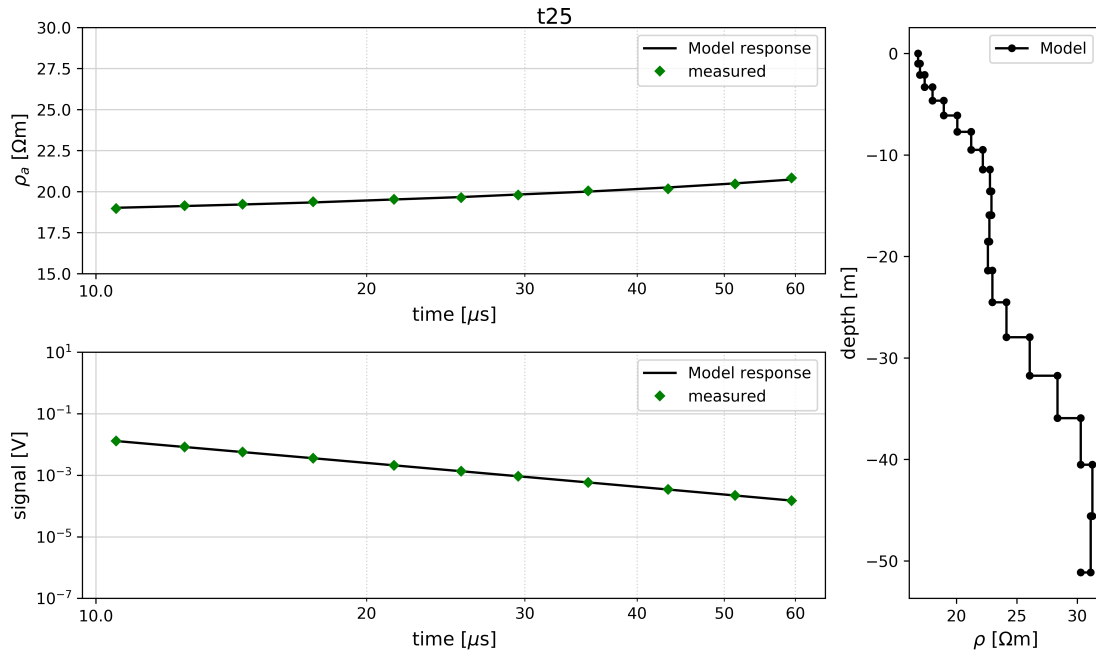


Figure 6.4: Raw data and forward modeling response of the resistivity/depth model on the right. The top left subplot shows the model response in terms of the apparent resistivity and the subplot below in terms of the measured secondary magnetic field.

The final inversion was done using data only from 10 to approximately 60 μs and an exemplary comparison to the measured data is shown in Figure 6.4. The green diamonds are indicating the selected subset, which was used for the inversion process. In this case the model response is a good representation of the measured data. In general, this holds true for most of the 86 soundings, except for a few soundings, which had to be filtered to an even narrower time window.

6.4 Results

6.4.1 Transient electromagnetic measurements

Figures 6.5, 6.6 and 6.7 show 2D sections of TEM-soundings along selected lines, which cross the landslide perpendicular from west to east. The single soundings were interpolated to obtain a color coded image of the subsurface. The locations of the soundings are indicated by the black rectangles within the figures.

The section shown in Figure 6.5 is located along ERT-profile QP2 and the distance along the profile is set according to the distance along the ERT-profile. The subsurface situation can be summarized by a 3-layer model:

1. The first layer extends to a depth between 10 and 15 m below the subsurface. It reveals a lateral less resistive anomaly at soundings 24 and 23.

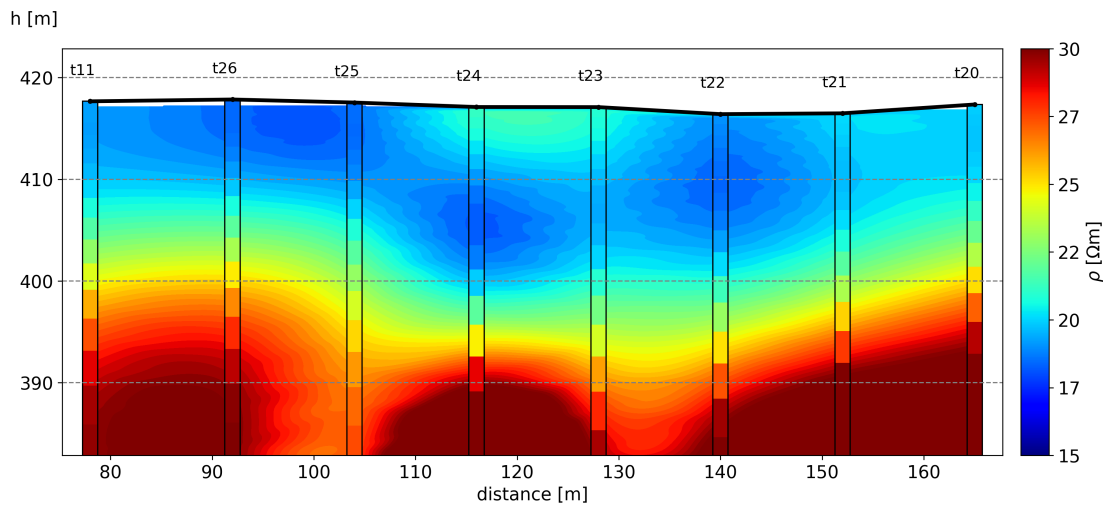


Figure 6.5: TEM-section along Line 2. The location is partly identical with ERT and SRT profile QP2 6.1 and starts at TEM-sounding number 11. The line ends with TEM-sounding number 20 in the west. The distance is chosen according to the distance along the QP2 ERT profile.

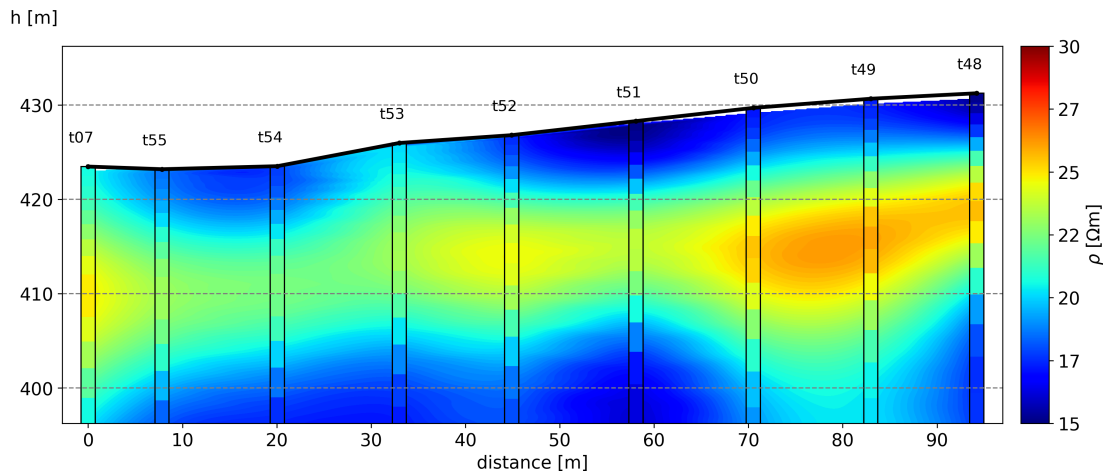


Figure 6.6: TEM-section along line 6. This line starts in the west of Figure 6.1 at TEM-sounding number 7 and ends with TEM-sounding number 48 in the east.

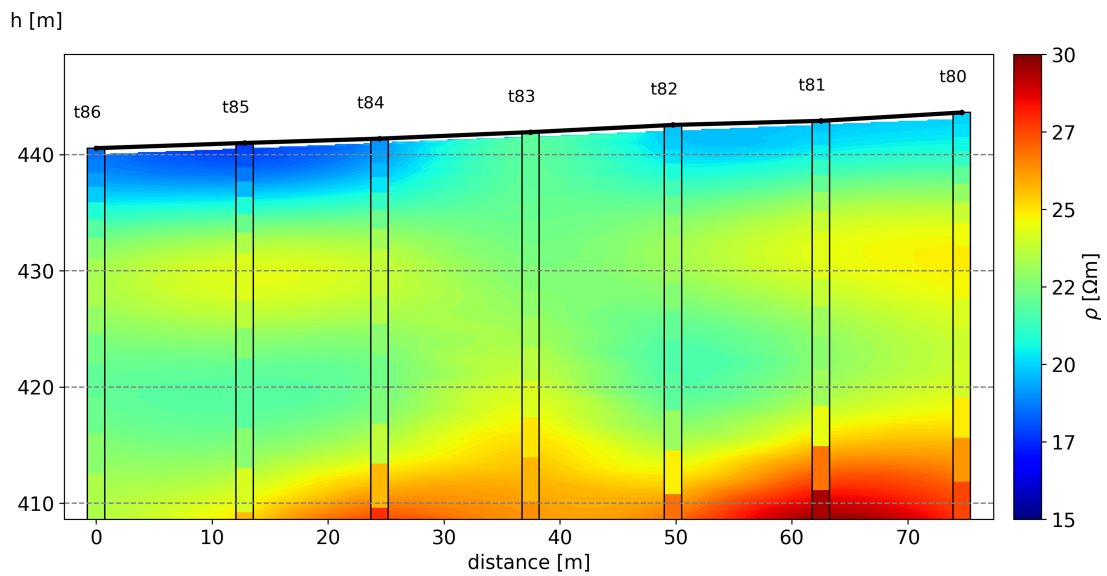


Figure 6.7: TEM-section along line 10. This line starts in the west of Figure 6.1 at TEM-sounding number 86 and ends with TEM-sounding number 80 in the east.

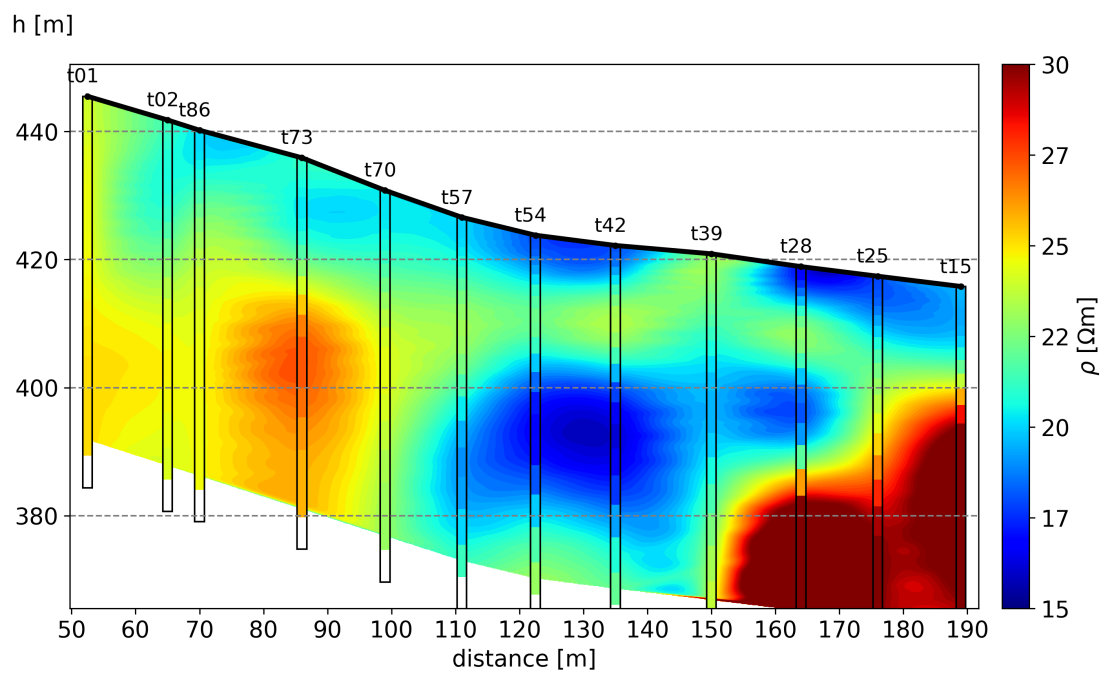


Figure 6.8: TEM – soundings along LP1 (ERT profile). This line starts in the south of Figure 6.1 at TEM-sounding number 1 and ends with TEM-sounding number 15 in the north. The distance is chosen according to the distance along the LP1 ERT profile.

2. The second layer is mainly a transition zone to higher resistivity, ranging between 15 and 20 m depth.
3. The bottom layer starts at 18 to 25 m depth and shows an increase to the highest resistivity at this site.

Figure 6.6 shows the subsurface below TEM-line 6, which is located in the middle of the landslide. Although the subsurface situation can be also described by a three layer model, the resistivity distribution is different compared to the situation presented in figure 6.5:

1. The first layer consists of materials with low electrical resistivity down to a depth of 2 m – 5 m.
2. The second layer consists mainly of materials with higher resistivity, down to a depth of approximately 20 m. This layer shows a high resistive anomaly in the latter part of the profile (soundings 50 to 48).
3. The bottom layer starts at a depth of approximately 20 m and shows low electrical resistivity, similar to the first layer.

Figure 6.7 shows the uppermost (in terms of height above sea level) TEM-line 10. This line is located outside of the active landslide area:

1. The first shallow layer is between 1 m and 3 m thick and exhibits the lowest electrical resistivity.
2. The second layer is between 15 m and 20 m thick and consists of materials with intermediate resistivity.
3. The third and bottom layer shows an increase to higher resistivity at a depth of 25 m to 30 m.

Figure 6.8 shows a TEM section that is orientated in the direction of the mass movement. This section is located along ERT-profile LP1. The subsurface situation can be described by an inhomogeneous 3-layer model:

1. The first layer consists of materials with intermediate to low electrical resistivity. This layer is between 1 m and 5 m thick.
2. The second layer is approximately 5 m thick and shows intermediate resistivity, but is not present continuously throughout the whole section. Especially, at the start (soundings 1, 2, 86) and end (soundings 25, 15) of the profile it merges with the third layer.
3. The third layer starts in a depth of approximately 20 m and shows the most inhomogeneous resistivity distribution. Intermediate to high resistivity is followed by low resistivity and at the end of the profile the highest resistivity can be observed.

Additionally the complete results are also presented in terms of 2D interpolated maps at certain depths below the subsurface (depth slices). The results at depths from 4 to 32 m in 4 m intervals below the subsurface can be found in Figure 6.9. Additionally the hill-shaded topographic model is shown in the top left corner. The colorbar at the right side of the Figure is valid for all 6 subplots and uses the same limits as the previous plots of the individual sections.

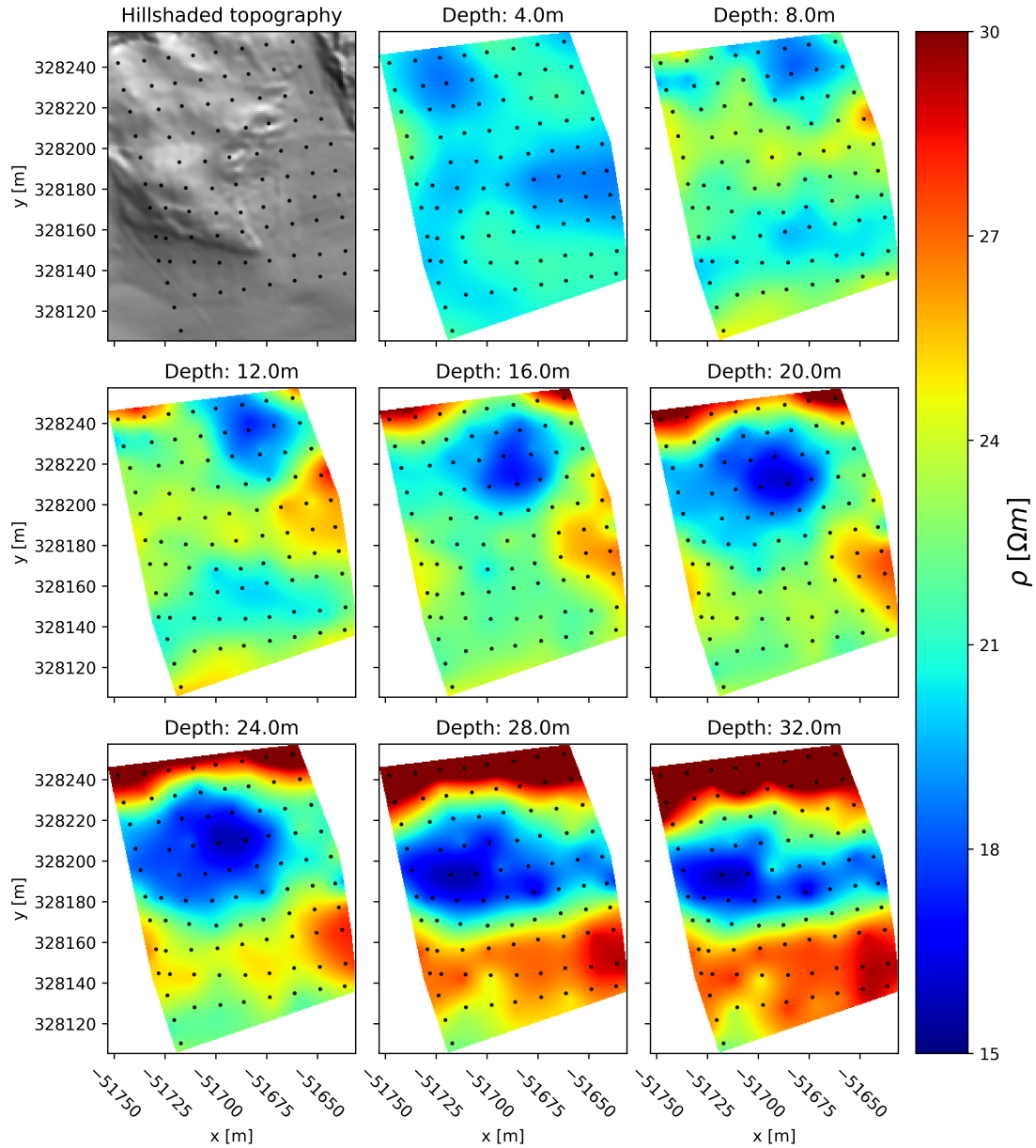


Figure 6.9: 2-D interpolation of the TEM 1-D models at selected depths. The black dots are indicating the center of sounding positions.

The first 3 depth slices (4, 8 and 12 m below the subsurface) show a transition to higher resistivity over the entire area, although there is a low resistive anomaly emerging in the north eastern part of the site. From depth slice 12 m to 24 m the low resistive anomaly increases gradually in size, until it shrinks again in depth slice 28 m and 32 m. The lowest depth slices (24, 28 and 32 m) show an emerging high resistive anomaly in the north of the landslide. Additionally, the resistivity values in the south of the site are also increasing, although not as high as in the northern part. In general, all resistivity anomalies are aligning partly with the topographic structures shown in the hill-shaded image in the top left corner.

6.4.2 Electromagnetic method at low induction number - Mapping

The electromagnetic measurements were initially visualized individually for each profile to assess the overall data quality and check for possible influence by metallic objects. Since the in-phase values (red lines in Figure 6.10) changes smoothly along most of the profiles it was possible to make sure that no metallic objects are located in the subsurface. Only a couple of measurements were heavily disturbed in some parts along the profile (an Example can be seen in Figure 6.11). The reason for this was already identified, during field acquisition, as the influence of the TEM-measurements. Due to time limitations TEM and EMI measurements were done parallel at the same time, but as soon as these issues were recognized the data acquisition was switched to alternating measurements between the two methods. In post processing the affected data was removed and the gaps were filled by interpolation.

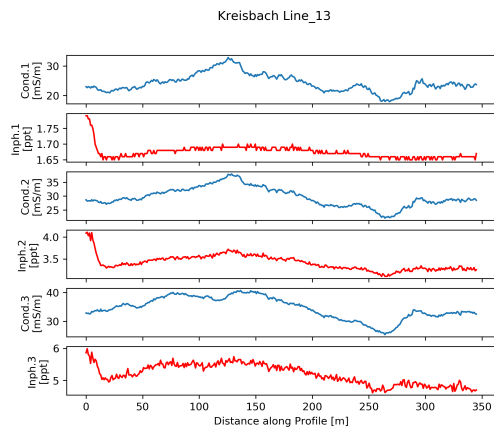


Figure 6.10: Raw-data plot of EMI line 13, which is exemplary of a clean measurement.

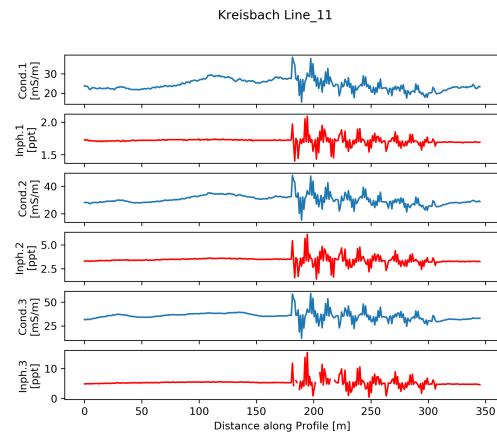


Figure 6.11: Raw-data plot of EMI line 11, which reveals the influence of parallel TEM-measurements at the end of the line.

The first two subplots of the top row of Figure 6.12 show the electrical resistivity (obtained from EMI conductivity via $\rho = 1/\sigma$) at 4.2 m and 6.7 m below the subsurface. Those measurements can be directly compared to the results from TEM soundings at

the same depths. Low resistive anomalies can be associated to higher clay content in the subsurface, which does not permit the water to flow quickly through these areas. Therefore, high resistive anomalies (higher sand content) can be associated with possible drainage systems, which permits the water to flow easier than in areas with higher conductivity. Both of those anomalies are partially consistent with the mean geomorphological features revealed by the hill-shaded digital elevation model (presented in the top right subplot of figure 6.12). Additionally, the high conductive anomalies also correlate well with areas where water is pooling after heavy precipitation events (from personal communication with the farmer).

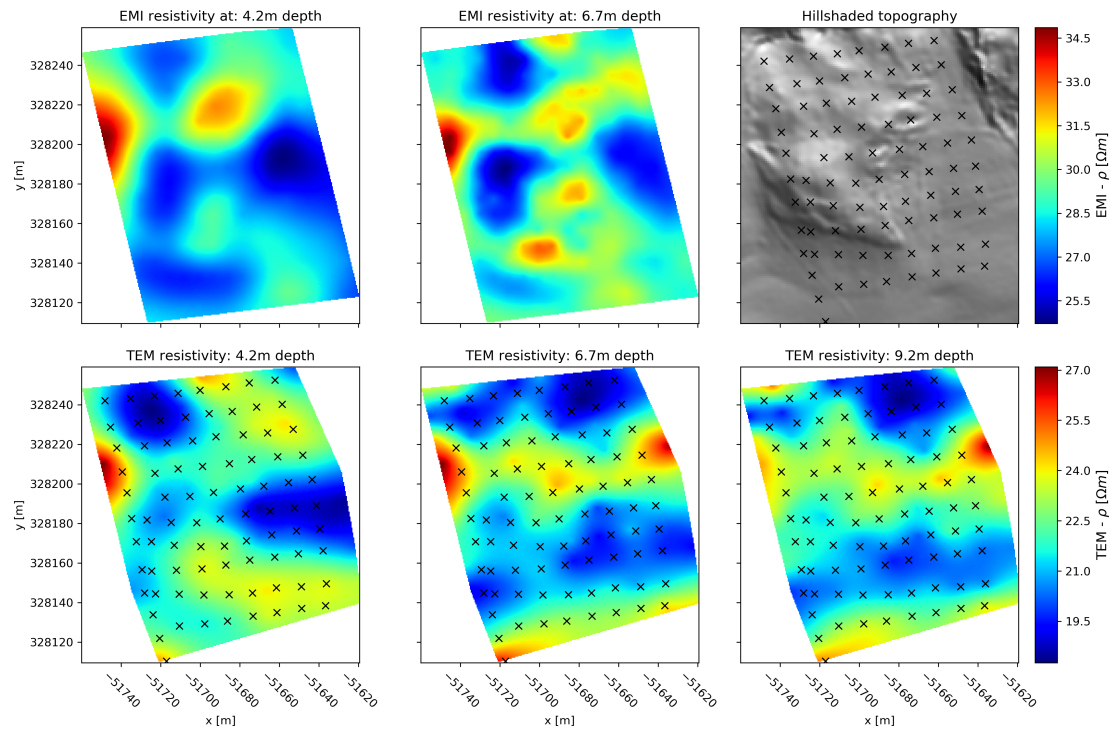


Figure 6.12: Comparison of EMI maps (top row), to TEM maps (bottom row), and to a hill-shaded topographic map (top right subplot).

6.4.3 Electrical resistivity and seismic refraction tomography for validation of the transient electromagnetic results

The results from ERT-measurements are shown in terms of electrical resistivity in figures 6.13 and 6.14 for the QP2 and LP1 profile respectively. The subplot on the right presents the comparison to results from TEM-soundings at a certain position indicated by the black rectangle within the ERT imaging section. Both lines are cropped to the extent of the respective TEM-lines, which were already presented in Figures 6.5 and 6.8. The comparison of the shapes of the 1-D models of electrical resistivity from ERT and TEM shows mainly consistent results, although there are some areas which also show

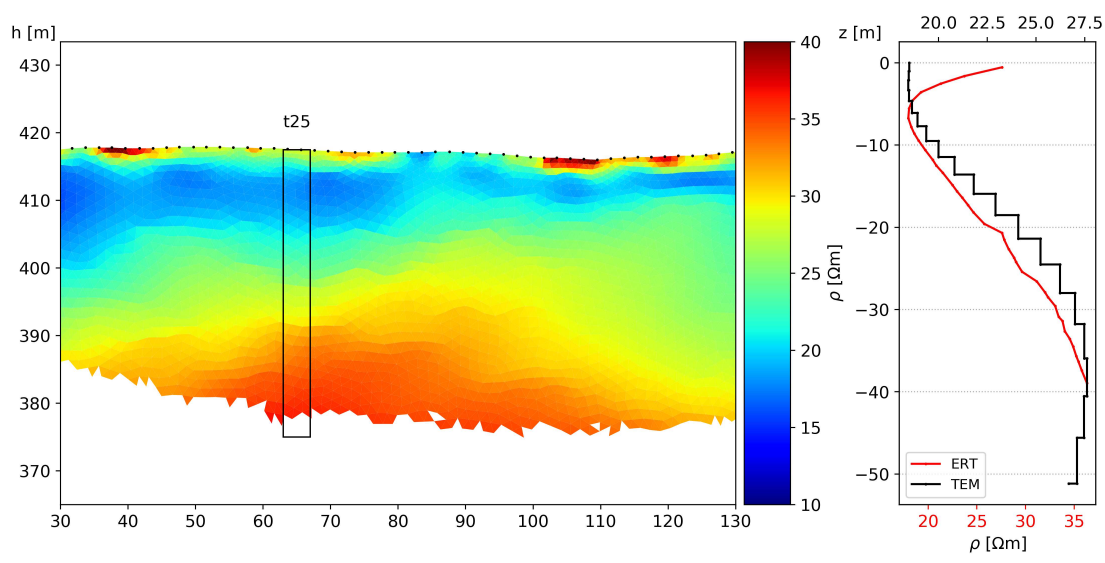


Figure 6.13: ERT profile qp2. The subplot on the right shows a comparison to a TEM sounding.

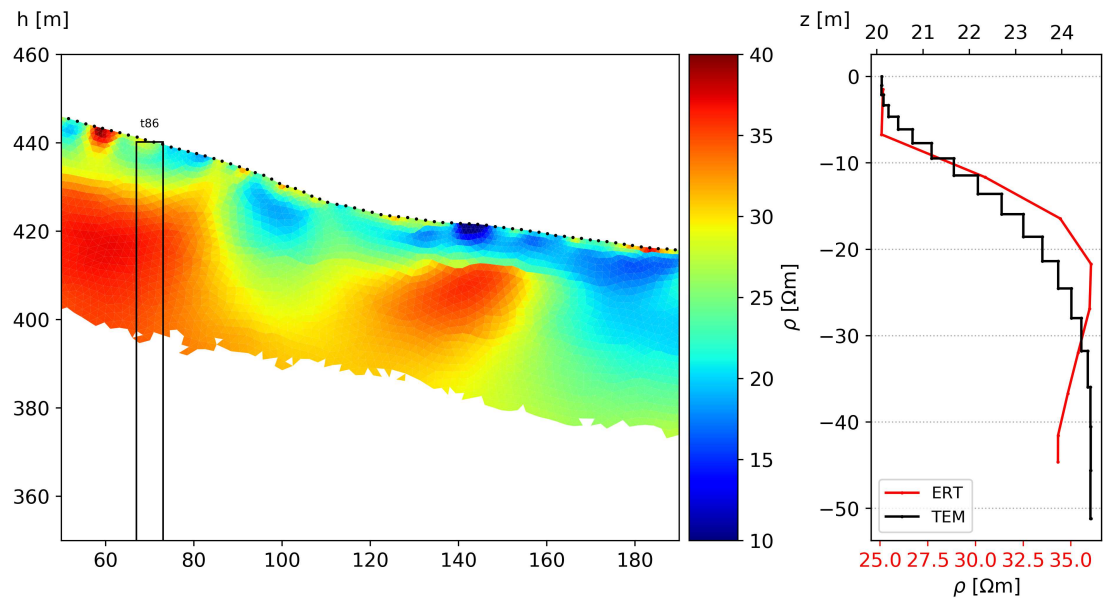


Figure 6.14: ERT profile lp1. The subplot on the right shows a comparison to a TEM sounding.

Kreisbach QP2: ERT vs SRT vs TEM

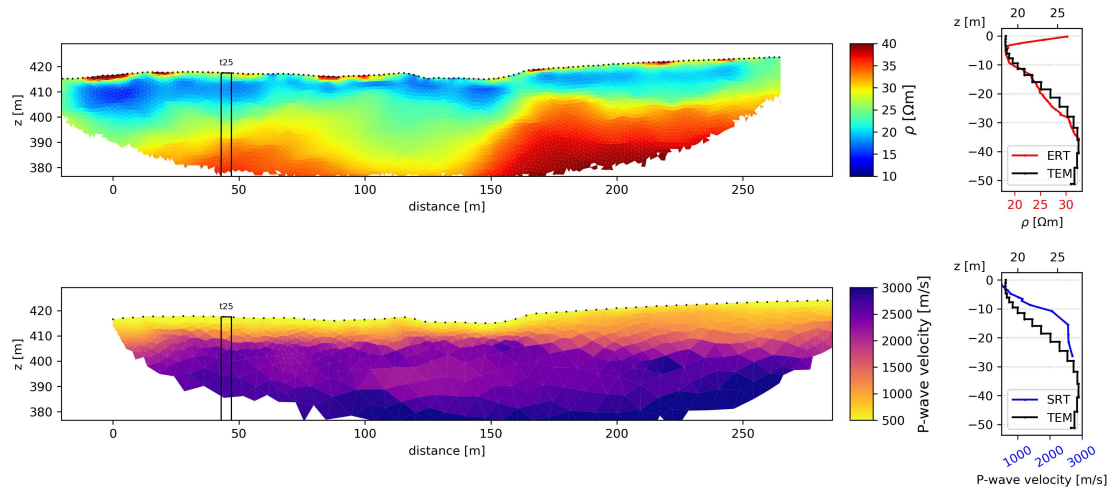


Figure 6.15: A comparison of results from ERT (top left subplot), SRT (bottom left subplot) and TEM measurements (right subplots) along QP2.

a significant offset between TEM-sections and ERT-sections. The values of the models vary over a much narrower range in case of the TEM measurements (ca. 15 - 30 Ωm), compared to values from ERT (10 - 40 Ωm).

The electrical resistivity of QP2, presented in Figure 6.13, shows a homogeneous image. The subsurface of QP2 can be described as a 3-layer model:

1. The shallow first layer (0 - 2 m depth) is consisting of laterally small scale high resistive anomalies.
2. This layer is followed by a low resistive layer to a depth of 10 m to 20 m.
3. The bottom layer is consisting of the highest resistivity, while its depth is varying from 30 m at the beginning of the profile to 40 m in the middle down to only 10 m at the end of the profile.

The comparison to a TEM sounding shows that the uppermost layer cannot be correctly solved by the TEM-method, but after that the shapes align almost perfectly.

The electrical resistivity of LP1, presented in Figure 6.14, shows a more heterogeneous subsurface image. Although the subsurface of LP1 can be described as a 3-layer model, lateral changes in the third layer can be observed. The transition from low resistivity to higher resistivity within the third layer are related to a change in lithology from higher clay content (lower resistivity) to higher sand content (higher resistivity). The results from TEM-measurements at LP1 (right subplot in Figure 6.14) are similar in shape and show the a similar transition to higher resistivity from 5 m to 25 m depth.

Figure 6.15 compares the results from SRT to ERT and TEM measurements at QP2. The subsurface situation as observed in the SRT-result can be described by a 4-layer model:

1. The first layer (0 - 5 m depth) shows the lowest seismic velocities up to 750 m/s, which are related to the most unconsolidated sediments.
2. The second layer (6 - 15 m depth) shows intermediate seismic velocities up to 1750 m/s, where the consolidation of the sediments increases.
3. The third layer (16 - 30 m depth) shows an increase of seismic velocities up to 2750 m/s, which are related to almost solid materials.
4. The bottom layer (31 - 40+ m depth) shows the highest seismic velocities up to 3500 m/s, which can be interpreted as the non-fractured bedrock.

The comparison to the ERT section above shows a general alignment of the 3-layer(ERT) and 4-layer(SRT) models, although the depression in the middle of the profile is more pronounced in the ERT image. Additionally, the uppermost layer is easier to distinguish in the ERT image, due to the stark contrast between shallow high resistive anomalies, to the low resistive second layer. Furthermore, the comparison to the TEM results shows an increase of resistivity from TEM sounding similar to the increase of seismic velocity from SRT.

6.5 Comparison to geotechnical methods and interpretation

The results from ERT, SRT and TEM are also compared to the dynamic probing and the core drilling at the intersection between LP1 and QP2, within figure 6.16. This comparison shows the classified core drilling results, the blow diagram from dynamic probing, the TEM 1-D log followed by a subplot containing both an extracted 1-D log from ERT and SRT at the position of interest.

Results from the core drilling were described by a geologist and classified to 5 classes as described within the legend of the first subplot from the left (Figure 6.16). These results can be summarized and described by a 3-layer model as follows:

1. The first layer is topped by a shallow layer of humus, followed by a couple of non-consolidated layers of clay and sandy sediments.
2. The second layer starts at approximately 5 m below the subsurface and consists of a similar mixture of clay and sand sediments, although the more consolidated (clay/silt hard) layers are more frequent and thicker.
3. The bottom layer starts at approximately 14 m below the subsurface and consists of consolidated clay stone.

The results from DPH testing are similar and can also be described by a 3-layer model as follows:

1. The first layer shows mainly a blow count smaller than 5 down to a depth of ca. 4 m.

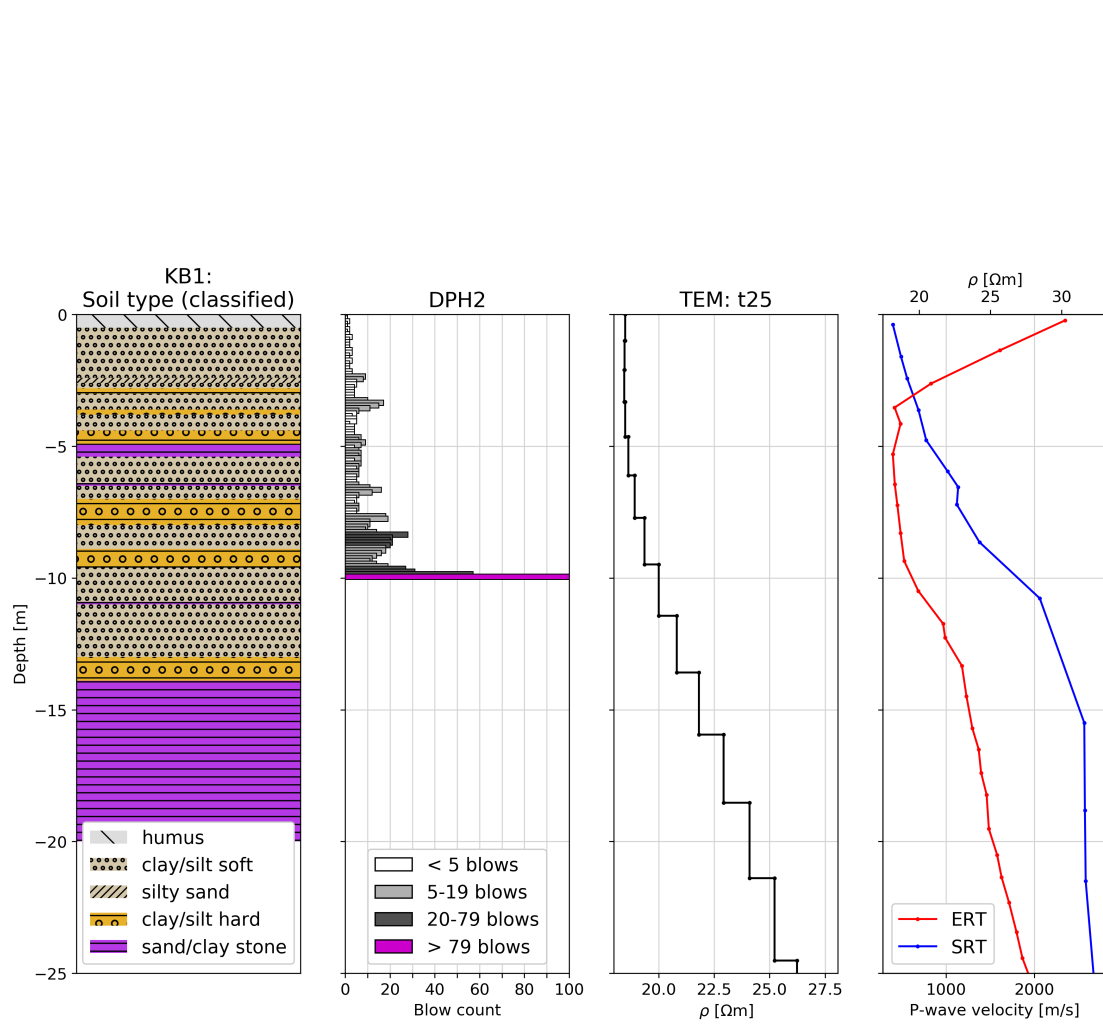


Figure 6.16: A comparison of results from geotechnical methods (1st and 2nd subplots) to geophysical methods (3rd and 4th subplot).

2. The second layer starts at approximately 5 m below the subsurface and shows a significant increase in blow counts higher than 5 and up to 20 blows per 10 cm.
3. The bottom layer starts at approximately 8 m below the subsurface and shows increasing blow counts over 20 blows until the metal rod got stuck at 10 m below the subsurface.

The comparison to results from geophysical can be also summarized by a 3-layer model as follows:

1. The first layer down to a depth of 5 m is consistent with seismic velocities up to 800 m/s and the transition from the highest electrical resistivity to the lowest within both the ERT and TEM model. However, the layer boundary in case of the TEM model is not as pronounced as in the ERT log.
2. The second layer stretches between 5 and approximately 15 m depth and is consisting of materials with seismic velocities between 850 m/s and 2500 m/s. This increase of seismic velocities is faster than within the first layer. The electrical resistivity obtained by TEM measurements show a slight increase between 5 m and 10 m depth.
3. The bottom layer starts at approximately 15 m below the subsurface and shows constant seismic velocities of approximately 2500 m/s. The electrical resistivity from both the ERT and TEM measurements are both gradually increasing below a depth of 10 m.

All these information allow the following interpretation of the landslide: The first layer consists of unconsolidated sand and clay minerals, which are most endangered of mass movements. The second layer is more stable than the first but still not completely consolidated and consists of a mixture of weathered clay- and sandstone. The depth to the bottom layer varies between 15 m and 35 m over the entire investigated area and can be described as the boundary to non-fractured clay- and sandstone. The discrimination between sandstone and claystone in the bottom layer is possible using the images of electrical resistivity obtained by both the ERT and TEM methods. High electrical resistivity is related to sandstone, and lower electrical resistivity to claystone.

6.6 Conclusion

This case study demonstrates that the Transient electromagnetic method is capable of providing additional as well as comparable information to help with the interpretation of other geophysical methods. Especially the comparison to near surface data from EMI mapping looks very promising and both methods supplement each other quite well. While the TEM-method provides information about deeper structures the EMI mapping is superior in terms of lateral near-surface resolution. Furthermore, high resolution data acquisition of EMI and TEM data of an area of approximately 100 m^2 was possible within a single day, by a team of 4 people.

The comparison to ERT and SRT measurements is mainly consistent, although an offset at some parts of the investigated area was observed. Similar to EMI and TEM, the ERT and TEM method also supplement each other well, while the ERT method is also able to provide information about deeper structures, which was extremely valuable for validation of the TEM data.

The comparison between geophysical and geotechnical methods shows that neither of those methods should be applied without each other, especially where the goal is to investigate larger areas with sufficiently fine resolution. Geophysical methods, while also providing additional information, are capable of filling the gaps between and extrapolating outside of geotechnical data. This is necessary and helpful, where steep topography and deep depth of interest would render sole application of geotechnical methods prohibitively expensive. Additionally the comparison of geophysical results to geotechnical ground truth data helped with the interpretation of the landslide. It was possible to distinguish between different lithological units by contrast within resulting subsurface images.

Future studies could use a combination of smaller and larger TEM loops to increase both the lateral resolution and the depth of investigation. Additionally it might be possible to improve the 1-D inversion of TEM measurements by taking the lateral changes of the subsurface properties below as well as in close vicinity of the TEM-loop into account and performing a 2-D or even a 3-D inversion of the measured data.

7 Conclusion

The main aim of this work was the quantification of the length of the turn-off ramp of the TEM-FAST 48 system. Based on oscilloscope measurements it was possible to visualize the processes within the transmitter loop, right after the current was shut off. This information was used to quantify the length of the ramp for different measurement setups, while providing an overview of the effect of different measurement setups on the length of the ramp. Additionally, the turn-off ramp times were used to improve the inversion results obtained with a commercial software.

To evaluate the improved inversion results two different near-surface case studies were done, which also provided the opportunity to emphasize the capabilities of the TEM method. Within the first one it was possible to validate the progression of a brick-clay resource outside of a currently excavated pit. The results were validated using the ERT method and the clay content measured from soil samples. The second case study was focused on the characterization of a clayey landslide by integral application of multiple geophysical methods. Through application of the TEM method it was possible to gain information on the distribution of electrical resistivity within a roughly $100 \times 100 \times 40 \text{ m}^3$ subsurface volume, using data collected within a single day by two people. The TEM results were compared to electrical resistivity obtained from EMI and ERT measurements and all three methods were able to obtain similar results. Additionally, the comparison to SRT measurements and geotechnical methods helped with the interpretation of the landslide.

The comparison of ramp measurements at two different sites suggests, that the influence of the subsurface resistivity on the length of the ramp is neglectable. Nonetheless, a forward modeling experiment has proven, that the effect of the turn-off ramp on the data is more pronounced for subsurfaces with higher resistivity. Therefore, and also to expand the existing data base of ramp measurements it might be interesting to measure the ramp at locations with even higher resistivity, such as permafrost sites. Additionally, it would be also rewarding for the author to take a look at constrained or even joint inversion of TEM data.

Bibliography

- Alex Kaminsky, (Zond software corporation). 2001. *Zondtem1d*. Version 28092019. <http://zond-geo.com/english/zond-software/electromagnetic-sounding/zondtem1d/>.
- Archie, Gustave E, et al. 1942. The electrical resistivity log as an aid in determining some reservoir characteristics. *Transactions of the AIME* 146 (01): 54–62.
- Auken, Esben, Nikolaj Foged, Jakob Juul Larsen, Knud Valdemar Trøllund Lassen, Pradip Kumar Maurya, Søren Møller Dath, and Tore Tolstrup Eiskjær. 2018. Ttem—a towed transient electromagnetic system for detailed 3d imaging of the top 70 m of the subsurface. *Geophysics* 84 (1): E13–E22.
- Boaga, Jacopo. 2017. The use of fdem in hydrogeophysics: a review. *Journal of Applied Geophysics* 139:36–46.
- Bücker, Matthias, Socorro Lozano Garcia, Beatriz Ortega Guerrero, Margarita Caballero, Liseth Pérez, Lizeth Caballero, Carlos Pita de la Paz, Alfredo Sánchez-Galindo, Francisco Jesús Villegas, Adrián Flores Orozco, et al. 2017. Geoelectrical and electromagnetic methods applied to paleolimnological studies: two examples from desiccated lakes in the basin of mexico. *Boletín de la Sociedad Geológica Mexicana* 69 (2): 279–298.
- Christiansen, Anders Vest, Esben Auken, and Kurt Sørensen. 2006. The transient electromagnetic method. In *Groundwater geophysics*, 179–225. Springer.
- Danielsen, Jens E, Esben Auken, Flemming Jørgensen, Verner Søndergaard, and Kurt I Sørensen. 2003. The application of the transient electromagnetic method in hydrogeophysical surveys. *Journal of applied geophysics* 53 (4): 181–198.
- Everett, Mark E. 2013. *Near-surface applied geophysics*. Cambridge University Press.
- Fitterman, David V, and Walter L Anderson. 1987. Effect of transmitter turn-off time on transient soundings. *Geoexploration* 24 (2): 131–146.
- Gonzalez-Alvarez, Ignacio. 2014. Landscape evolution as the contextual key feature for greenfields geochemical exploration in regolith-dominated terrains: the albany-fraser orogen-yilgarn craton margin, western australia. In *2014 gsa annual meeting in vancouver, british columbia*.
- Jones, Eric, Travis Oliphant, Pearu Peterson, et al. 2001. *SciPy: open source scientific tools for Python*. [Online; accessed]. <http://www.scipy.org/>.

- Kemna, Andreas. 2000. *Tomographic inversion of complex resistivity: theory and application*. Der Andere Verlag.
- Knödel, Klaus, Heinrich Krummel, and Gerhard Lange. 2013. *Handbuch zur erkundung des untergrundes von deponien und atlasten: band 3: geophysik*. Springer-Verlag.
- Marchant, David. 2015. Induced polarization effects in inductive source electromagnetic data. PhD diss., University of British Columbia.
- Murphy, BS. 2014. Pykrige: development of a kriging toolkit for python. In *Agu fall meeting abstracts*.
- Paxton, Stan. 2016. *Answer to: two reasons why porosity is important in the production of oil*. Online; accessed October 10, 2019. <https://www.quora.com/Why-is-porosity-important-in-the-production-of-oil>.
- Raiche, AP. 1984. The effect of ramp function turn-off on the tem response of layered earth. *Exploration Geophysics* 15 (1): 37–41.
- Rücker, Carsten, Thomas Günther, and Florian M. Wagner. 2017. pyGIMLi: an open-source library for modelling and inversion in geophysics. *Computers and Geosciences* 109:106–123. ISSN: 0098-3004. doi:10.1016/j.cageo.2017.07.011. <http://www.sciencedirect.com/science/article/pii/S0098300417300584>.
- Schnabel, W., J. Schweigl, K. Grösel, H.G. Krenmayr, and C. Rupp. 2013. Exkursion e3 – flysch- und klippenzone, rutschungen und massenbewegungen in der flysch-zone der blätter 55 ober-grafendorf und 56 st. pölten. *Arbeitstagung der Geologischen Bundesanstalt*.
- Slater, Lee, AM Binley, W Daily, and Richard Johnson. 2000. Cross-hole electrical imaging of a controlled saline tracer injection. *Journal of applied geophysics* 44 (2-3): 85–102.
- Spies, Brian R. 1989. Depth of investigation in electromagnetic sounding methods. *Geophysics* 54 (7): 872–888.
- Telford, William Murray, WM Telford, LP Geldart, Robert E Sheriff, and RE Sheriff. 1990. *Applied geophysics*. Vol. 1. Cambridge university press.
- Ward, Stanley H, and Gerald W Hohmann. 1988. Electromagnetic theory for geophysical applications. In *Electromagnetic methods in applied geophysics: voume 1, theory*, 130–311. Society of Exploration Geophysicists.
- Waxman, Monroe H, LJM Smits, et al. 1968. Electrical conductivities in oil-bearing shaly sands. *Society of Petroleum Engineers Journal* 8 (02): 107–122.